Chronic stress induces significant gene expression changes in the prefrontal cortex alongside alterations in adult hippocampal neurogenesis

Short title: Transcriptomic effects of chronic stress

Ksenia Musaelyan[1,5], Selin Yildizoglu[1], James Bozeman[1], Andrea Du Preez[1, 2, 3], Martin Egeland[1, 2, 3], Patricia A Zunszain[2], Carmine M Pariante[2], Cathy Fernandes,[3,4] and Sandrine Thuret [1]*

1. Department of Basic and Clinical Neuroscience, Institute of Psychiatry, Psychology and Neuroscience, King's College London, London, UK
2. Department of Psychological Medicine, Institute of Psychiatry, Psychology and Neuroscience, King's College London, London, UK
3. Social, Genetic and Developmental Psychiatry Centre, Institute of Psychiatry, Psychology and Neuroscience, King's College London, London, UK
4. MRC Centre for Neurodevelopmental Disorders, King's College London, London, UK
5. Department of Physiology, Anatomy and Genetics, University of Oxford, Oxford UK

*Corresponding authors: ST (Sandrine.1.thuret@kcl.ac.uk)

Keywords: chronic stress, gene expression, adult hippocampal neurogenesis, prefrontal cortex

Abstract

Adult hippocampal neurogenesis is involved in stress related disorders such as depression, posttraumatic stress disorders, as well as in the mechanism of antidepressant effects. However, the molecular mechanisms involved in these associations remain to be fully explored. In this study, unpredictable chronic mild stress in mice resulted in a deficit in neuronal dendritic tree development and neuroblast migration in the hippocampal neurogenic niche. To investigate molecular pathways underlying neurogenesis alteration, genome-wide gene expression changes were assessed in the prefrontal cortex, hippocampus and the hypothalamus alongside neurogenesis changes. Cluster analysis showed that the transcriptomic signature of chronic stress is much more prominent in the prefrontal cortex compared to the hippocampus and the hypothalamus. Pathway analyses suggested huntingtin, leptin, myelin regulatory factor, methyl-CpG binding protein and brain derived neurotrophic factor as the top predicted upstream regulators of transcriptomic changes in the prefrontal cortex. Involvement of the satiety regulating pathways (leptin) was corroborated by behavioural data showing increased food reward motivation in stressed mice. Behavioural and gene expression data also suggested circadian rhythm disruption and activation of circadian clock genes such as Period 2. Interestingly, most of these pathways have been previously shown to be involved in the regulation of adult hippocampal neurogenesis. It is possible that activation of these pathways in the prefrontal cortex by chronic stress indirectly affects neuronal differentiation and migration in the hippocampal neurogenic niche via reciprocal connections between the two brain areas.

Abbreviations

ACC- anterior cingulate cortex

Ascl1 - Achaete-scute homolog 1

Bdnf - Brain Derived Neurotrophic Factor

CNTRL - control

CRP – C-reactive protein

DBS- deep brain stimulation

DCX - doublecortin

DEG – differentially expressed genes

DG – dentate gyrus

FDR - false discovery rate

GM-CSF - granulocyte-monocyte colony stimulating factor

GZ – granular zone

HIP - hippocampus

HPA – hypothalamo-pituitary-adrenal axis

Htt - Huntingtin

Iba1 - Ionized calcium binding adaptor molecule 1

IFNγ - interferon gamma

IL - interleukin

IPA – Ingenuity Pathway Analysis

Lep - Leptin

Mecp2 - Methyl-CpG Binding Protein 2

Mtor – mechanistic target of rapamycin

Myrf - Myelin Regulatory Factor

NF-kB - nuclear factor kappa B

NSF – novelty suppressed feeding

PFA - paraformaldehyde

PFC- prefrontal cortex

PST – Porsolt swim test

SAM – statistical analysis of microarrays

SGZ – subgranular zone

TNFα - tumour necrosis factor alpha

UCMS- unpredictable chronic mild stress

Introduction

Adult hippocampal neurogenesis is thought to play an important role in depression and antidepressant effects (Boldrini *et al*., 2019; Egeland *et al*., 2017; Miller and Hen, 2015), however its exact role in the course of disease neurobiology is unknown. Chronic stress has been identified as a significant risk factor for depression (Bernet and Stein, 1999; Fava and Kendler, 2000; Pawlby *et al*., 2011). Unpredictable chronic mild stress (UCMS) is widely used as a valid model of depression. UCMS induces such behavioural endophenotypes as anhedonia, anxiety, decreased grooming and weight loss (Ducottet *et al*., 2004; Mutlu *et al*., 2012; Nollet *et al*., 2013). However some groups report hyperactivity and anxiolytic effect of this paradigm (Pothion *et al*., 2004; Schweizer *et al*., 2009; Strekalova *et al*., 2011). UCMS is also associated with a decline in hippocampal neurogenesis. While multiple hypotheses have been put forward to explain the mechanism of neurogenic decline (Egeland *et al*., 2015), a full coherent clinically relevant picture has not yet been formed. One of the ways to study neurobiological mechanisms in their full complexity is to utilise hypothesis-free explorative approach of a genome-wide transcriptome changes in selected tissues and brain regions. This approach is currently being widely utilised in clinical depression research to discover novel genes and pathways involved in the neurobiology of depression (Cattaneo *et al*., 2018; Hervé *et al*., 2017).

The majority of the research on depression and chronic stress focuses on the brain areas of the cortico-limbic circuit, including but not limited to the hippocampus, hypothalamus and the prefrontal cortex (PFC). Human neuroimaging studies confirm the involvement of these regions in depression (Lorenzetti *et al*., 2009; van Tol *et al*., 2014). The role of PFC in depression is further supported by the evidence from the deep brain stimulation (DBS) trials, showing that DBS over PFC and ACC produces an antidepressant effect (Berlim *et al*., 2014; Levkovitz *et al*., 2009). Investigation of PFC pathology in animal models of depression demonstrated that exposure to chronic stress and increased glucocorticoid levels cause damage and neurodegenerative changes in the PFC, such as appearance of reactive microglia (Hinwood *et al*., 2013), atrophy of pyramidal neurons (Cerqueira, 2005), dendritic atrophy (Dias-Ferreira *et al*., 2009; Liston *et al*., 2006) and reduction of synaptic proteins expression and synaptic currents (Li *et al*., 2011; Muller *et al*., 2011).

Yet the majority of transcriptomic studies of chronic stress effects in rodents focused on the consequence of stress on gene expression in the hippocampus. The hippocampus has been shown to be particularly sensitive to stress, potentially due to a high expression of the glucocorticoid receptor (GR) activated by corticosteroid hormone released in the course of stress response. Both rat and mouse studies find activation of immune response-related gene networks and signalling pathways often centred around nuclear factor kappa B (NF-kB) (Gray *et al*., 2014; Malki *et al*., 2013, 2015). A number of other studies investigating the effect of chronic mild or restraint stress on hippocampal gene

expression in rats and mice identified signalling pathways involved in cell fate, such as cell apoptosis (Bergström *et al*., 2007), proliferation and cell cycle control (Liu *et al*., 2010), axonal guidance and cell migration (Datson *et al*., 2012; Jungke *et al*., 2011; Zitnik *et al*., 2013).

Another region of interest in the chronic stress research is the hypothalamus. As a central organ in the hypothalamo-pituitary-adrenal (HPA) axis regulating the systemic level of glucocorticoids, hypothalamus plays a central role in the endocrinal stress response of the body. Hypothalamus also receives neuroendocrine input from the gut metabolic hormones ghrelin and leptin and is connected with the reward related ventral tegmental area (van Zessen *et al*., 2012). Another hypothalamic area implicated in chronic stress response is the suprachiasmatic nucleus, a major regulator of the circadian clock, relevant for sleep disturbance and alteration of molecular circadian rhythms observed in depression (Li *et al*., 2013).

For these reasons, the three limbic circuit brain areas described above were selected in this study to analyse genome-wide transcriptomic changes induced by UCMS exposure to find novel potential mechanisms of stress-induced neurogenic decline using a hypothesis-free approach.

Materials and Methods

Experimental design

7 weeks old male BALB/cAnNCrl mice were obtained from Charles River (Margate, Kent, U.K.). All mice were housed in the Biological Services Unit at the Institute of Psychiatry, Psychology & Neuroscience in standard conditions (19-22°C, humidity 55%, 12h:12h light:dark cycle with lights on at 7.30am, food [Rat and Mouse No. 1 Diet; Special Diet Services, Essex, UK] and water ad libitum). Mice were allowed to acclimatise to new housing conditions for 1 week before experimental procedures commenced. All housing and experimental procedures were carried out in compliance with the local ethical review panel of King's College London under a U.K. Home Office project licence held in accordance with the Animals (Scientific Procedures) Act 1986 and the European Directive 2010/63/EU.

Two cohorts of 8 weeks old male BALB/c mice were exposed to UCMS or control (CNTRL) conditions. Mice were randomly allocated to experimental groups. The BALB/c strain was selected for this study due to its high sensitivity to stress and high immune system reactivity (Kim *et al*., 2002; Potter, 1985; Surget and Belzung, 2009). The first cohort was sacrificed for tissue collection after 6 weeks of UCMS exposure to examine the behavioural changes and the state of the hippocampal neurogenic niche (n=10 per group). As the behavioural data from Cohort 1 demonstrated the strongest behavioural phenotype at week 4, Cohort 2 was sacrificed for tissue collection after 4 weeks of UCMS exposure to detect UCMS-induced gene expression events potentially preceding changes in the adult hippocampal neurogenesis (n=8 per group). For graphical representation of the study design see Supplementary Figure 1.

UCMS protocol and behavioural assessments

The UCMS protocol used was based on the methodology described by Nollet *et al*., (2013). The UCMS group was exposed to four daily stressors in a random-like order repeated every week. In order to avoid habituation, the longevity of stressors varied from 30 min on week 1 to 4 hours towards the end of the UCMS protocol. For the schedule of stressors included in the protocol see Supplementary Methods Table 1.

Animals' weight and coat state were assessed during UCMS on a weekly basis. Coat score was determined on a scale of zero to seven according to Nollet *et al*., (2013) by a researcher blinded to experimental conditions. Sucrose preference test was conducted during and at the end of the UCMS exposure. The following additional tests were conducted at the end of the UCMS exposure: open field, novelty suppressed feeding (NSF), splash test, Porsolt swim test (PST). For the details of experimental procedures see Supplementary Methods.

Blood collection

For cytokine and corticosterone analysis blood was collected by incision method from the lateral tail vein (Sadler and Bailey, 2013) 24 hours before and 30 minutes after the PST. Whole blood (30-50 µL) was collected into EDTA microvette CB 300 tubes (Sarstedt, Leicester, UK) and separated by centrifugation for 10 min at 3000 rpm (4°C). Blood was also collected by the cardiac puncture after terminal general anaesthesia has been induced. 100-200 µL of whole blood was collected using syringe injected into the cardiac cavity and subsequently processed as described above. This blood draw was used for cytokine, C-reactive protein (CRP) and leptin measurements.

Corticosterone measurement

Plasma corticosterone levels were measured using a commercially available corticosterone enzyme-linked immunosorbant assay kit (ELISA, Enzo Life Sciences, Lausen, Switzerland) according to the manufacturer's instructions for small sample volume. All samples were analysed in technical duplicates. Obtained data was analysed using five parameter logistic curve analysis using the My Assays online data tool, MyAssays Ltd., http://www.myassays.com/five-parameter-logistic-curve.assay.

Luminex

The level of cytokines in the plasma was determined using the multiplex screening assay based on magnetic Luminex® xMAP® technology as described in Hye *et al*. (2014). For this assay custom-made pre-mixed multianalyte kit was purchased from RnD systems, Minneapolis, USA (catalogue N LXSAMSM). This kit contained multi-coloured magnetic microparticles pre-coated with antibodies to 10 selected analytes (granulocyte-monocyte colony stimulating factor (GM-CSF), interleukins IL-1β, IL-2, IL-4, IL-5, IL-6, IL-10, tumour necrosis factor alpha (TNFα) and interferon gamma (IFNγ), CRP and leptin. To

measure the fluorescent signal Luminex® 100/200™ system was used. All assay steps were conducted according to the manufacturer instructions. Due to the small volume of blood collected, technical replicates for plasma samples were not included. Obtained data was analysed using five parameter logistic curve analysis using the My Assays online data tool, MyAssays Ltd., http://www.myassays.com/five-parameter-logistic-curve.assay.

Brain tissue collection

To collect fixed tissue, animals were anaesthetised with Euthatal i.p. (Merial Animal Health Ltd, Harlow, UK) at a dose of 40 mg/kg pentobarbital sodium. Deep anaesthesia was confirmed by the loss of righting and pain reflexes and slowing of the rate of respiration. Animals were subsequently transcardially perfused with 30ml of saline and 50ml of 4% paraformaldehyde (Paraformaldehyde, prills, 95%, 441244, Sigma-Aldrich, Poole, UK) in phosphate-buffered saline (pH = 7.4 from PBS tablets, 18912-014, Gibco by Life Technologies, Paisley, UK) through the left cardiac ventricle. Brains were post-fixed overnight in 4% PFA at 4°C for 24 hours, and subsequently stored at 4°C in 30% sucrose (Sigma-Aldrich, Poole, UK) in PBS until sectioning (1-3 weeks).

For fresh frozen tissue collection, following decapitation brains were removed from the skull and placed dorsal side down on a wetted filter paper on a petri dish kept on ice. For the dissection of the brain areas technique see Supplementary methods. Right and left dissected areas were pooled for each sample, while brain tissue from each mouse was analysed as individual samples. Dissected brain areas were immediately flash frozen on dry ice.

Immunohistochemistry

Serial coronal sections of 40µM thickness were cut on a HM430 sliding freezing microtome (Thermo Scientific) and stored in tris-buffered saline (TBS, pH=7.4) with 30% v/v glycerol, 15% w/v sucrose and 0.05% w/v sodium azide (all Sigma Aldrich, UK). For immunohistochemistry on free floating sections every sixth section was used. Immunohistochemistry was conducted as previously described (Dias, Bevilaqua, *et al*., 2014). For neuroblast detection anti-DCX antibody (Ab18723 raised in rabbit, Abcam, UK, 1:1000 dilution) was used; for microglia immunostaining antibody for Iba1 (019-19741, Wako, Japan, 1:500 dilution) was used.

Stereological analysis of immunopositive cell density

For microscopy, the Axioskop 2 MOT Plus Miscroscope (Zeiss) with automated stage connected to Stereoinvestigator v.7 (MBF Bioscience, US) software was used. Immunopositive cell density was determined using the volume and cell population number estimated by semi-automated Optical Fractionator method applied by the stereological software (see Supplementary Methods). All quantifications were done by an experimenter blinded to the experimental conditions.

DCX cell classification based on dendrite morphology and their morphometric analysis

The DCX positive cells were visually classified according to the categorization of Plümpe *et al*. (2006). EF-type neurons from each section were selected for morphometric analysis of dendrites. For this, sections were imaged using a 40× objective, and micrographs were acquired using a Zeiss AxioCam MR Rev3 camera. Primary, secondary and tertiary dendrites were manually traced using the NeuronJ plugin for ImageJ developed by Meijering et al., (2004) and measured using image pixel to mm calibration as has been done previously (Dias, Bevilaqua, *et al*., 2014; Srivastava *et al*., 2012). For details see Supplementary methods.

Migration distance of DCX+ cells

To estimate relative distance of DCX+ cells migration through the granular zone, the height of the GZ has been divided into ten bins, and a relative distance of migration was estimated by assigning a score from 0 to 1 to each DCX+ cell based on the position of its cell body relative to the borders of the GZ as has been done previously (Han *et al*., 2016). The average percentage of cells positioned within each distance bin for each brain was used in statistical analysis.

Microarray and data analysis

Genome-wide gene expression was assessed in fresh frozen brain tissue using the Mouse WG-6 BeadChip Kit (Illumina, US) (for details of RNA extraction see Supplementary Methods). Eight brains were sampled for each treatment condition; no technical replicates were utilised. Sample labelling, hybridisation and signal detection and imaging were performed according to manufacturer's instructions. Images were analysed using the GenomeStudio software (Illumina, US). Raw data was pre-processed using the R package Lumi (Du *et al*., 2008). Statistical analysis of differential expression was performed using the Statistical Analysis of Microarrays (SAM) method and R-based software (Tusher *et al*., 2001). The dataset for each brain region was analysed separately as a two-class unpaired data. For further details see Supplementary methods. Microarray data analysis was verified using real-time quantitative PCR (qPCR). For gene selection, primer design and qPCR see Supplementary Methods.

Statistical analysis

Unpaired two-tailed t test was used for between group comparisons after normal distribution of the data was confirmed with the Kolmogorov-Smirnov test for single measures. For the weekly coat state between group comparisons Mann-Whitney U-test used for each week as the data was not normally distributed. For related measures, such as DCX+ cells, dendritic morphology types and migration distance groups two-way ANOVA was used with post-hoc Bonferroni multiple comparisons within each type or distance group.

Data availability

Output of SAM analysis for each brain region is available in the Supplementary materials for this article. Raw microarray output data is available on request.

Results

UCMS impaired coat state and grooming behaviour in exposed mice

UCMS induced significant coat state deterioration detectable from week 4 of stress exposure (Mann-Whitney for week 4 $U = 2$ $p < 0.0001$, for week 5 $U = 21$ $p = 0.023$, for week 6 $U = 9$ $p = 0.004$) (see Figure 1A). Repeated measures 2-way ANOVA showed that body weight of animals was significantly affected by week of exposure (Effect of Time $F (6, 108) = 127.2$ $p < 0.0001$) and UCMS X Time interaction ($F (6, 108) = 5.026$ $p = 0.0001$) (see Figure 1B). Sucrose consumption, measured once every 2 weeks, was significantly decreased in UCMS group compared to control only on week 4 when sucrose concentration was increased from 1% to 2% (see Figure 1C). The control group responded to 2% sucrose with 79% preference, while the UCMS-exposed group did not prefer it over water (46%) (Effect of Time x Stress $F (3, 39) = 13.15$, $p < 0.0001$). In the splash test UCMS-exposed mice spent shorter time grooming ($t (18) = 3.304$, $p= 0.004$) (see Figure 1D). UCMS also induced hyperactivity in the open field test (see Figure 1E) (Mann-Whitney $U = 16$, $p = 0.009$). In the NSF test UCMS-exposed group's latency to feed was reduced compared to control group (unpaired two-tailed t-test $t (18) = 3.227$, $p = 0.005$) (see Figure 1F). No differences were found in the time of immobility on the PST (see Figure 1G).

UCMS did not affect plasma corticosterone response to acute swim stress but increased plasma CRP and reduced plasma leptin levels

To analyse the HPA axis regulation of glucocorticoid release in response to stressful stimulation, blood samples were collected 24 hours before and 30 min after a 6 minutes long PST. Corticosterone levels were significantly elevated after PST in both groups but UCMS did not affect the baseline level of CORT or response to swim stress (Effect of PST $F (1, 16) = 108.6$, $p< 0.0001$) (see Figure 1H). None of the ten cytokines, measured at the time of sacrifice, were detected in the plasma. However, CRP was significantly elevated in the UCMS group ($t (16) = 2.508$, $p = 0.023$) (see Figure 1I). Leptin levels, reflecting hormonal regulation of appetite, were significantly decreased in UCMS group compared to controls ($t (14) = 2.477$, $p = 0.027$) (see Figure 1J).

UCMS reduces the density of mature DCX+ neuroblasts and the percentage of DCX+ cells residing in the SGZ

UCMS group presented with a reduced number of DCX+ neuroblasts in the hippocampal dentate gyrus (DG) ($t (14) = 2.954$, $p=0.01$) (see Figure 2D). Density reduction was specific to neuroblasts with mature-

like dendritic trees reaching into the molecular layer of the DG (type "EF" in Plümpe *et al*., 2006). See Figure 2D for quantification and 2E for examples of each neuroblast type.

As adverse environment has been previously shown to affect migration of the adult-born neuroblasts (Belarbi et al., 2012), the effect of the UCMS on migration distance of the DCX+ cells was analysed (Effect of Interaction $F(10,170) = 1.99$, $p = 0.037$; Effect of distance $F(10,170) = 622$, $p<0.0001$). UCMS reduced the percentage of DCX+ cells residing in the SGZ ($p = 0.005$), see Figure 2B for examples and 2A for quantification. However, the average relative distance of migration of DCX+ cell bodies from the SGZ was not significantly different between the two groups (see Figure 2C).

UCMS does not affect the number of Iba1+ microglia in the hippocampal GZ, but increases its density in the medial PFC

Analysis of Iba1+ microglial density showed that no significant effect of UCMS on the number of microglial cells was found (see Figure 2F and 2G). However, density of Iba1+ microglia was increased in the medial PFC of the UCMS-exposed group compared to control ($t(16) = 3.139$, $p=0.006$) (see Figure 2H and 2I).

UCMS exerted the strongest effect on gene expression in the PFC

To elucidate molecular pathways underlying UCMS effects, bulk genome-wide gene expression analysis of the brain tissue was conducted using the gene expression microarray. For this, a separate cohort of mice (Cohort 2) was exposed to UCMS or control conditions (n=8 per group). As behavioural monitoring during 6 weeks of UCMS exposure in Cohort 1 showed the strongest phenotype on week 4 (see Figure 1A and C), this time point was chosen for gene expression analysis. Behavioural assessment preceded tissue collection at week 4. Behavioural data confirmed the presence of low grooming and hyperactivity phenotypes seen in Cohort 1, however some differences where observed in the dynamics of sucrose preference response (see Supplementary figure 2).

Hierarchical cluster analysis based on the top 500 variable genes showed that samples primarily clustered based on the brain region they derived from, while within the regions some treatment group – based clustering was observed. The PFC samples clustered based on the UCMS exposure, apart from two outlier samples which were excluded from subsequent analysis as shown in Figure 3. In the hippocampus only few control and UCMS-exposed samples clustered together, and no clear distinct pattern of expression could be seen on the heatmap for the hippocampal (HIP) UCMS and CNTRL samples. In the hypothalamus no clustering based on stress exposure was observed (see Figure 3).

Differential expression analysis using SAM package yielded the highest number of significant genes in the PFC

Significance Analysis of Microarrays (SAM) method detected 467 differentially expressed genes (DEGs) between the UCMS and CNTRL groups in the PFC with FDR of 0. For the full list of top up- and downregulated genes selected based on their fold changes see Supplementary data table 4. As such a low level of FDR was calling a very small number of genes in other regions, FDR level was relaxed to a recommended 0.095 for the hippocampus and the hypothalamus. Such settings called 46 and 27 differentially expressed genes in the hippocampus and in the hypothalamus respectively (see Supplementary Table 5).

Pathway analysis revealed meaningful pathways, functions and predicted upstream regulators in the PFC dataset

Canonical pathway analysis conducted by the IPA™ software mapped the DEGs on known canonical pathways. The software identified a total of 240 canonical pathways associated with the DEGs. Among these 17 were statistically significant ($p<0.05$) based on Fisher's exact test analysis utilised by the IPA (see Table 1). The software also quantified the ratio of the number of DEGs involved in each pathway to the total number of genes comprising the pathway. Table 1 lists all DEGs involved in each of the significantly activated pathways. Based on the fold changes of the DEGs, IPA also made a prediction of whether the pathway would be up (positive Z-score) or down (negative Z-score) regulated and its magnitude (Z-score value). Due to conflicting direction of DEGs change in some pathways it was not always possible to make such a prediction (missing Z-score). Interestingly a pathway directly related to axonal maturation, the axonal guidance pathway was identified as the most significant. The list also included pathways previously shown to be involved in neurogenesis regulation such as Wnt/ β-catenin and Ephrin signalling. Common pathways of neuronal signalling such as glutamate, calcium and GABA receptor signalling were also identified. Interestingly, immune response related B cell receptor pathway also appeared to be significantly activated.

Table 1 Canonical pathways deemed significant in the PFC dataset by IPA pathway analysis
Canonical pathways deemed significant in the PFC dataset ordered by the log (p-value) derived from Fisher's exact test, with dataset genes/pathway genes ratio and z-score of predicted pathway up or downregulation, calculated for pathways where differential gene expression showed consistent direction of change

INGENUITY CANONICAL PATHWAYS	-LOG (P-VALUE)	RATIO	Z-SCORE	ASSOCIATED DIFFERENTIALLY EXPRESSED GENES
Axonal Guidance Signalling	2.61	0.05	-	Ephb2, Tuba4a, Gng13, Sema4f, Robo3, Gng7, Tubb2b, Ephb6, Sema6d, Mag, Wnt10a, Efna5, Arhgef6, Lingo1, Mras, Myl4, Fzd5, Sema7a, Adamts4

Glutamate Receptor Signalling	2.12	0.10	-	Slc17a7, Slc17a6, Homer1, Grm4, Gng7
Calcium Signalling	2.03	0.06	2.45	Camk2a, Tnnc1, Myh3, Rcan3, Myl4, Mef2c, Itpr1, Camkk2, Camk2g
Wnt/β-catenin Signalling	2.01	0.06	0.33	Csnk2a2, Nlk, Wnt10a, Dkk3, Sox10, Fzd5, Acvr2b, Sox11, Tcf7l2
GABA Receptor Signalling	1.94	0.09	-	Slc32a1, Gabrg1, Gad1, Mras, Ap2s1
Paxillin Signalling	1.65	0.07	0.45	Actn2, Actb, Arhgef6, Mras, Itgb4, Mapk11
Thrombin Signalling	1.64	0.05	1.89	Camk2a, Arhgef6, Mras, Myl4, Gng13, Itpr1, Mapk11, Gng7, Camk2g
Gαq Signalling	1.63	0.06	1.13	Napepld, Adrbk1, Mras, Gng13, Arhgef25, Itpr1, Chrm3, Gng7
Ephrin B Signalling	1.50	0.07	-	Ephb6, Ephb2, Mras, Gng13, Gng7
RhoGDI Signalling	1.49	0.05	-0.82	Dgkz, Arhgdig, Actb, Arhgef6, Mras, Myl4, Gng13, Gng7
B Cell Receptor Signalling	1.40	0.05	2.12	Synj2, Map3k10, Camk2a, Inpp5f, Mras, Mef2c, Mapk11, Camk2g
CCR5 Signalling in Macrophages	1.35	0.08	-	Mras, Gng13, Mapk11, Gng7
G Protein Signalling Mediated by Tubby	1.34	0.09	-	Mras, Gng13, Gng7
Triacylglycerol Degradation	1.33	0.14	-	Faah, Mgll
α-Adrenergic Signalling	1.31	0.06	-	Adra2a, Mras, Gng13, Itpr1, Gng7
Glutamate Dependent Acid Resistance	1.30	0.50	-	GAD1

Next, the predicted upstream regulators analysis was conducted using the IPA software. Upstream regulator analysis identifies molecules which activation or suppression can explain gene expression changes in the dataset, as well as regulators' own interactions with each other. The software utilises a broad definition of the upstream regulator for this analysis, so that any type of regulatory molecule, from microRNA to a drug, can be included in the results. IPA identified 63 potential upstream regulators of DEGs, with 59 being significant according to Fisher exact test. Table 2 lists the top 15 predicted upstream regulators with p value less or equal to 0.01, connected to two or more differentially expressed genes. In some cases, the software could also make a prediction of the direction and

magnitude of up- or downregulation based on the fold changes data available for target genes (activation z-score).

Table 2 Upstream regulators of differentially expressed genes in the PFC dataset predicted by the IPA software. IPA pathway analysis predicted upstream regulators in the PFC dataset, p value derived from Fisher exact test. Z-score reflects the direction of change where the software was able to make such a prediction.

	UPSTREAM REGULATOR	GENE NAME	ACTIVATION Z-SCORE	P-VALUE	N OF TARGET GENES
1	Htt	Huntingtin	-0.004	0.0000	25
2	Lep	leptin	-0.970	0.0000	8
3	Myrf	myelin regulatory factor		0.0001	3
4	Mecp2	methyl-CpG binding protein 2	1.126	0.0001	7
5	Bdnf	brain-derived neurotrophic factor	-0.181	0.0001	9
6	Hdac4	histone deacetylase 4		0.0001	8
7	Kmt2a	lysine methyltransferase 2A	1.342	0.0002	5
8	Ntrk2	neurotrophic receptor tyrosine kinase 2		0.0011	3
9	Dcc	DCC netrin 1 receptor		0.0018	2
10	Pou4f1	POU class 4 homeobox 1		0.0022	4
11	Comt	catechol-O-methyltransferase		0.0035	2
12	Mtor	mechanistic target of rapamycin		0.0054	3
13	Arntl	aryl hydrocarbon receptor nuclear translocator like		0.0117	2
14	Ascl1	achaete-scute family bHLH transcription factor 1		0.0123	3
15	Bckdk	branched chain ketoacid dehydrogenase kinase		0.0153	2

Figure 4 highlights several key upstream regulators with the most number of target genes (Huntingtin (Htt), Leptin (lep), Myelin Regulatory Factor (Myrf), Methyl-CpG Binding Protein 2 (Mecp2) and Brain Derived Neurotrophic Factor (Bdnf)) at the centre of the regulatory network, as well as the predicted complexity of their regulatory relationships with the DEGs and among themselves. According to the analysis Htt was identified as the leading regulator, with 25 DEGs from the PFC dataset listed as its target genes. Leptin, Mesp2, Bdnf and Hdac4 followed huntingtin with seven to nine target genes among the DEGs. Some of the top upstream regulators could be grouped into three main categories: those previously implicated in neurogenesis regulation (Bdnf, Mtor, Ascl1), those involved in

epigenetic regulation (Mecp2 and Hdac4) and those related to some of the observed behaviours (Htt, Lep). The relationships between the main upstream regulators and their differentially expressed target genes are shown in Figure 4. Colour coding reflects direction of fold change of the DEGs (red for upregulation and green for downregulation). Interestingly, most upstream regulators were not themselves differentially expressed, with the exception of BAF Chromatin Remodeling Complex Subunit B (Bcl11b), which was downregulated. In the hippocampus and the hypothalamus, the number of genes was not sufficient to produce meaningful results in the pathway analysis.

Functional analysis identified functions related to dendritic morphology

Next, we assessed if differentially expressed genes in the PFC dataset were linked to particular functions in the IPA database. IPA identified 185 functions related to the DEGs. The most relevant functions, based on their relation to the brain, the number of associated DEGs and their activation z-score are listed in Table 3. These functions fell in the main three groups: those related to synaptic plasticity, such as long-term potentiation or synaptic depression, those related to dendritic morphology, such as neurite formation or neuritogenesis and branching of neurites, and those related to cell fate such as cell proliferation, differentiation and migration. Overall, functions related to cellular and nervous system development dominated the list.

Table 3 Predicted functions associated with the differentially expressed genes in the PFC dataset.
Gene functions predicted by IPA software and selected based on their relevance for the brain, number of genes related to each function and the ability of the software to make a prediction regarding the direction of change (activation z-score).

CATEGORIES	FUNCTIONS ANNOTATION	P-value	Activa-tion z-score	N of genes
Cell-To-Cell Signaling &Interaction	long-term potentiation of brain	0.005	-1.177	9
	long-term potentiation of cerebral cortex	0.007	-0.923	8
	neurotransmission	0.009	-0.164	8
	long-term potentiation	0.013	-0.978	10
	release of neurotransmitter	0.016	-1.718	4
	synaptic depression	0.031	-0.527	6
Cell Morphology, Cellular Assembly & Organization, Cellular Development, Cellular Function & Maintenance, Cellular Growth & Proliferation, Embryonic Development, Nervous System	branching of neurites	0.004	-0.250	13
	neuritogenesis	0.004	-0.250	15
	dendritic growth/branching	0.008	-1.342	11
	outgrowth of neurites	0.050	1.898	6

Development & Function, Tissue Development				
Cellular Assembly & Organization, Cellular Development, Cellular Growth & Proliferation, Nervous System Development & Function, Tissue Development	microtubule dynamics	0.003	-0.346	17
	growth of neurites	0.039	2.129	8
Cellular Development, Cellular Growth & Proliferation, Nervous System Development & Function, Tissue Development	proliferation of neuronal cells	0.013	0.995	11
	development of neurons	0.001	0.017	20
Cellular Growth & Proliferation	proliferation of cells	0.002	0.512	27
	generation of cells	0.000	0.101	22
Cellular Development	differentiation of cells	0.001	0.460	19
Lipid Metabolism, Molecular Transport, Small Molecule Biochemistry	concentration of lipid	0.007	-2.400	7
Nervous System Development & Function, Tissue Morphology	density of neurons	0.014	-2.213	7
Developmental Disorder, Neurological Disease, Organismal Injury & Abnormalities	cerebral dysgenesis	0.024	0.931	4
Behavior	Behavior	0.037	0.687	8
Cellular Movement, Nervous System Development & Function	migration of neurons	0.050	-0.124	6

Discussion

In this study adult male BALB/c mice were exposed to 6 weeks of UCMS conditions, which resulted in low grooming, hyperactivity, transient anhedonia, and change in food reward behaviour in UCMS-exposed mice. Behavioural changes were accompanied by increase in CRP and decrease in leptin plasma levels, reactive microglia changes in the PFC area, and decline in the number of neuroblasts and their aberrant migration in the granular zone of the hippocampal dentate gyrus.

UCMS is known to induce a complex behavioural response, with our study being no exception. As expected, UCMS consistently reduced grooming in mice. Hyperactivity was also very prominent, in line

with many previous UCMS studies (Couch *et al*., 2013; Dournes *et al*., 2013), especially where the stressors are administered in the light phase and therefore likely disrupt the circadian rhythm of mice (Aslani *et al*., 2014). Hyperactivity following UCMS has been previously linked to impulsivity (Couch *et al*., 2016). Contrary to expectations, UCMS-exposed mice demonstrated decreased latency to feed in the NSF test. There are several possible explanations for this effect. Firstly, it could be simply linked to hyperactivity in the UCMS group. Secondly, it is possible that UCMS stimulated food reward drive in mice. Such explanation goes in line with a decline in blood leptin in the UCMS group. Leptin is a negative feedback inhibitor released by adipose tissue to regulate food consumption through leptin receptors in the hypothalamus (Ahima and Osei, 2004), thus its reduction could lead to a higher drive for food rewards. Such effect of chronic stress on leptin levels has been previously documented (Ge *et al*. (2013) Liu *et al*. (2015). Importantly, calorie intake and satiety regulating hormones are known to modulate adult neurogenesis (Garza *et al*., 2012; Hornsby *et al*., 2016; Morgan *et al*., 2017). Change in leptin levels might be reflecting a shift in circadian rhythm which could have affected the time of feeding drive and levels of hormones regulating it, as has been shown in previous studies of circadian rhythm gene knockouts or mice exposed to disrupted light-dark cycles (Kettner *et al*., 2015).

Lastly, it has been shown previously that mouse response in the NSF test is dependent on the ambiguity of the previous experience of aversive stimuli and the state of adult hippocampal neurogenesis. Glover *et al*., (2017) demonstrated that neurogenesis-deficient mice which undergone ambiguous cue fear conditioning training, showed lower latency to feed in the NSF test compared to their neurogenesis-intact counterparts. This effect was attributed to the failure of neurogenesis deficient mice to generalise the aversive experience to novel environments. Due to the unpredictable nature of UCMS, it could have exerted an effect similar to ambiguous cue and led to analogous deficiency of fear generalisation in the NSF arena. While fear conditioning paradigm differs significantly from the UCMS and their underlying mechanisms might not overlap, it is still interesting to consider that anomalous NSF response in neurogenesis-deficient mice has been described previously.

To investigate molecular changes which underlie this combination of endophenotypes associated with chronic stress exposure, we used a hypothesis-free approach of genome-wide gene expression microarray. As behavioural monitoring showed the strongest stress behavioural response at 4 weeks, this time point was selected for gene expression analysis. A number of differences were observed in behavioural response between the two cohorts, which could be attributed to the difference in the length of UCMS exposure and variable nature of UCMS protocol well described in the literature (Willner, 2005).

Potential expression changes were assessed in areas previously involved in chronic stress response, such as hippocampus, the hypothalamus and the PFC. Interestingly, genome wide gene expression changes

were most apparent in the PFC among the three regions investigated, with no overlap among the regions. This finding goes in line with previous studies which compared the effect of chronic mild stress on gene expression across different brain regions. As such, Herve *et al*. (2017) found the strongest effect on UCMS in anterior cingulate cortex compared to the dentate gyrus, with only five overlapping DEGs between the two regions. Similarly, Surget *et al*. (2008) reported less DEGs in the dentate gyrus upon UCMS compared to amygdala and the cortex, with the cortex response being more broad in terms of cellular functions involved. Interestingly, the RNAseq study conducted by Nollet *et al*. (2019) showed much more overlap between hippocampus and the prefrontal cortex upon UCMS exposure. It is possible that the differences in the methodology of this paper (surgery was conducted on all mice prior to UCMS; older age of mice at the start of UCMS; higher sensitivity of the RNAseq compared to microarray approach) could explain variation in results. Nonetheless, a strong gene expression response of the PFC to the UCMS exposure is a common finding among all studies and has been confirmed by our results. The lack of hippocampal response can be explained by the fact that UCMS mostly induces affective, not cognitive symptoms in mice, which would be expected to correlate with hippocampal response.

Many target genes, upstream regulators and signalling pathways involved in the PFC response in our study could be linked to dendritic remodelling and spine atrophy, a well-described effect of chronic stress on the PFC. Based on the IPA pathway and upstream regulator analysis, glutamatergic and calcium signalling, as well as Htt and Bdnf-centred networks stood out as the most significantly involved. Indeed, repeated stress is known to cause suppressed glutamate receptor expression and signalling in the PFC, which is thought to be linked to dendritic atrophy (Yuen *et al*., 2012). Many recent studies have explored the antidepressant potential of ketamine in chronic stress animal models of depression, strengthening the glutamatergic theory of depression (Sun *et al*., 2016; Zhu *et al*., 2015). In addition, disruption of glutamatergic signalling has been previously linked to hyperactivity (Procaccini *et al*., 2011). Calcium signalling has also been implicated in dendrite remodelling, via its effect on protein kinase A (PKA) and protein kinase C (PKC). Calcium is a necessary cofactor in the activation of PKA and PKC, and it has been shown that pharmacological suppression of the PKA and PKC activation prevented spine atrophy following chronic stress exposure (Hains *et al*., 2009, 2015).

The limited number of differentially expressed genes in the hippocampus did not permit carrying out pathway analyses. It is possible that the lack of differential gene expression detection comes from the heterogeneity of the dorsal and ventral hippocampal tissue, which were pulled together in this study. Alternatively, this could be a limitation of a time point of tissue collection, as the mice displaying neurogenesis changes were exposed to the UCMS for two weeks longer than the mice from which tissue for gene expression analysis was derived. However, it is also conceivable that the activation of the signalling pathways affecting dendritic morphology in the PFC has a downstream indirect effect on hippocampal neurons via PFC-hippocampal connections. Indeed, PFC and the hippocampus are known

to be connected via multiple direct and indirect pathways, mostly involved in memory functions (Eichenbaum, 2017). This notion is supported by the enrichment of cell proliferation, differentiation and migration functions in the functional analysis of the PFC dataset. Indeed UCMS reduced dendritic length in PFC as well as in the hippocampus in a previous study (Morais *et al*., 2017). Importantly, in line with our findings, this study also showed that dendritic tree alterations were associated with a more pronounced decrease in neuroplasticity related gene expression in the PFC compared to the hippocampus. Interestingly, PFC-hippocampus connections have been previously implicated in food reward related behaviour (Hsu *et al*., 2018). In addition, increased functional connectivity in the prefrontal cortex areas and the hippocampus among other limbic structures were associated with sleep disruption in people reporting depressive problems (Cheng *et al*., 2018). Dendritic tree and dendritic spine density measurements in the PFC and the hippocampus could show if these molecular changes led to dendritic morphology alteration in adult neurons in these two regions.

Similarly, microglial cell density was increased in the PFC but not the hippocampus of the UCMS-exposed mice. While appearance of reactive microglia upon chronic stress has been described to take place simultaneously in the hippocampus and the PFC (Wohleb *et al*., 2012), previous studies also suggested that the PFC is more sensitive to chronic stress than the hippocampus (Yuen *et al*., 2012). At the same time PFC has been shown to be less prone to microglial dystrophy following chronic stress, which could also explain the presence of microglial increase at the time of sacrifice only in this area (Kreisel *et al*., 2014). Interestingly however, inflammatory pathways did not come up in the gene expression analysis. This could be related to the length of UCMS exposure prior to frozen tissue harvesting, as most previous studies collected tissue after 7 to 9 weeks of UCMS schedule as opposed to 4 weeks in our study.

Finally, our genome-wide gene expression analyses suggested the involvement of two mechanisms not predicted from the behavioural or immunohistochemical experiments carried out in this project, namely the modulation of myelination by Myrf and epigenetic pathways regulated by Mecp2. Future myelin measurements and epigenetic regulation assays could show if indeed UCMS caused any functional changes in these domains.

To conclude, UCMS induces major gene expression changes in the PFC which could potentially underlie UCMS-associated deficiency in the adult hippocampal neurogenesis. Glutamatergic and calcium signalling, leptin signalling, as well as Htt and Bdnf-regulated networks were identified as the main pathways involved. These gene expression changes preceded changes in food reward behaviour, increase in microglia density in the PFC and a decline in the number of neuroblasts in the hippocampal dentate gyrus, as well as their aberrant migration through the granular zone. These findings highlight the heterogeneous neurobiological effects of the chronic stress exposure which could lead to depression-like phenotype.

Funding

This study was funded by Janssen Pharmaceutica. KM and ADP were funded by Janssen Pharmaceutica Studentships.

Competing interests

This study was funded by Janssen Pharmaceutica to develop a model to test novel strategies for the treatment of depression which are being developed by the company. SY, JB, ME, ST, PAZ, CMP and CF declared no potential conflicts of interest with respect to the research, authorship, and/or publication of this article.

Acknowledgements

The authors would like to thank the MRC Social, Genetic and Developmental Psychiatry Centre research facility for conducting the microarray detection and Abdul Hye, PhD for help with the Luminex technology.

References

Ahima RS and Osei SY (2004) Leptin signaling. *Physiology and Behavior* 81(2): 223–241.

Ambrogini P, Lattanzi D, Ciuffoli S, Agostini D, Bertini L, Stocchi V, Santi S and Cuppini R (2004) Morpho-functional characterization of neuronal cells at different stages of maturation in granule cell layer of adult rat dentate gyrus. *Brain Research* 1017(1–2): 21–31.

Aslani S, Harb MR, Costa PS, Almeida OFX, Sousa N and Palha JA (2014) Day and night: diurnal phase influences the response to chronic mild stress. *Frontiers in Behavioral Neuroscience* 8: 82.

Bagot RC, Cates HM, Purushothaman I, Lorsch ZS, Walker DM, Wang J, Huang X, Schlüter OM, Maze I, Peña CJJ, Heller EAA, Issler O, Wang M, Song W, Stein JL, Liu X, Doyle MA, … Nestler EJ (2016) Circuit-wide Transcriptional Profiling Reveals Brain Region-Specific Gene Networks Regulating Depression Susceptibility. *Neuron*: 1–15.

Belarbi K, Arellano C, Ferguson R, Jopson T and Rosi S (2012) Chronic neuroinflammation impacts the recruitment of adult-born neurons into behaviorally relevant hippocampal networks. *Brain, Behavior, and Immunity* 26(1): 18–23.

Bergström A, Jayatissa MN, Thykjær T and Wiborg O (2007) Molecular Pathways Associated with Stress Resilience and Drug Resistance in the Chronic Mild Stress Rat Model of Depression—a Gene Expression Study. *Journal of Molecular Neuroscience* 33(2): 201–215.

Berlim MT, McGirr A, Van Den Eynde F, Fleck MPA and Giacobbe P (2014) Effectiveness and acceptability of deep brain stimulation (DBS) of the subgenual cingulate cortex for treatment-resistant depression: A systematic review and exploratory meta-analysis. *Journal of Affective Disorders* 159: 31–38.

Bernet CZ and Stein MB (1999) Relationship of childhood maltreatment to the onset and course of major depression in adulthood. *Depression and Anxiety* 9(4): 169–174.

Boldrini M, Galfalvy H, Dwork AJ, Rosoklija GB, Trencevska-Ivanovska I, Pavlovski G, Hen R, Arango V and Mann JJ (2019) Resilience Is Associated With Larger Dentate Gyrus, While Suicide Decedents With Major Depressive Disorder Have Fewer Granule Neurons. *Biological Psychiatry*, Elsevier.

Cattaneo A, Ferrari C, Uher R, Bocchio-Chiavetto L, Riva MA and Pariante CM (2016) Absolute measurements of macrophage migration inhibitory factor and interleukin-1-β mRNA levels accurately predict treatment response in depressed patients. *International Journal of Neuropsychopharmacology* 19(10): 1–10.

Cattaneo A, Cattane N, Malpighi C, Czamara D, Suarez A, Mariani N, Kajantie E, Luoni A, Eriksson JG, Lahti J, Mondelli V, Dazzan P, Räikkönen K, Binder EB, Riva MA and Pariante CM (2018) FoxO1, A2M, and TGF-β1: three novel genes predicting depression in gene X environment interactions are identified using cross-species and cross-tissues transcriptomic and miRNomic analyses. *Molecular Psychiatry*, Nature Publishing Group 23(11): 2192–2208

Cerqueira JJ (2005) Morphological Correlates of Corticosteroid-Induced Changes in Prefrontal Cortex-Dependent Behaviors. *Journal of Neuroscience* 25(34): 7792–7800.

Cheng W, Rolls ET, Ruan H and Feng J (2018) Functional Connectivities in the Brain That Mediate the Association Between Depressive Problems and Sleep Quality. *JAMA Psychiatry* 75(10): 1052.

Chomczynski P and Sacchi N (1987) Single-step method of RNA isolation by acid guanidinium thiocyanate-phenol-chloroform extraction. *Analytical Biochemistry*, Academic Press 162(1): 156–159.

Couch Y, Anthony DC, Dolgov O, Revischin A, Festoff B, Santos AI, Steinbusch HW and Strekalova T (2013) Microglial activation, increased TNF and SERT expression in the prefrontal cortex define stress-altered behaviour in mice susceptible to anhedonia. *Brain, Behavior, and Immunity* 29: 136–146.

Couch Y, Trofimov A, Markova N, Nikolenko V, Steinbusch HW, Chekhonin V, Schroeter C, Lesch K-P, Anthony DC and Strekalova T (2016) Low-dose lipopolysaccharide (LPS) inhibits aggressive and augments depressive behaviours in a chronic mild stress model in mice. *Journal of Neuroinflammation*, Journal of Neuroinflammation 13(1): 108.Datson NA, Speksnijder N, Mayer JL, Steenbergen PJ, Korobko O, Goeman J, de Kloet ER, Joëls M and Lucassen PJ (2012) The transcriptional response to chronic stress and glucocorticoid receptor blockade in the hippocampal dentate gyrus. *Hippocampus* 22(2): 359–371.

Dias-Ferreira E, Sousa JC, Melo I, Morgado P, Mesquita AR, Cerqueira JJ, Costa RM and Sousa N (2009) Chronic Stress Causes Frontostriatal Reorganization and Affects Decision-Making. *Science* 325(5940): 621–625.

Dias GP, Bevilaqua MC do N, Da Luz ACDS, Fleming RL, De Carvalho LA, Cocks G, Beckman D, Hosken LC, De Sant'Anna Machado W, Corrêa-e-Castro AC, Mousovich-Neto F, De Castro Gomes V, Bastos G de NT, Kubrusly RCC, Da Costa VMC, Srivastava D, Landeira-Fernandez J, … Gardino PF (2014) Hippocampal biomarkers of fear memory in an animal model of generalized anxiety disorder. *Behavioural Brain Research* 263: 34–45.

Du P, Kibbe WA and Lin SM (2008) lumi: A pipeline for processing Illumina microarray. *Bioinformatics* 24(13): 1547–1548.

Ducottet C and Belzung C (2005) Correlations between behaviours in the elevated plus-maze and sensitivity to unpredictable subchronic mild stress: Evidence from inbred strains of mice. *Behavioural Brain Research* 156(1): 153–162.

Ducottet C, Aubert A and Belzung C (2004) Susceptibility to subchronic unpredictable stress is related to individual reactivity to threat stimuli in mice. *Behavioural Brain Research* 155(2): 291–299.

Dulawa SC and Hen R (2005) Recent advances in animal models of chronic antidepressant effects: The novelty-induced hypophagia test. *Neuroscience & Biobehavioral Reviews*, Pergamon 29(4–5): 771–783.

Dournes C, Beeské S, Belzung C and Griebel G (2013) Deep brain stimulation in treatment-resistant depression in mice: Comparison with the CRF1 antagonist, SSR125543. *Progress in Neuro-Psychopharmacology and Biological Psychiatry*, Elsevier Inc. 40: 213–220.

Egeland M, Zunszain PA and Pariante CM (2015) Molecular mechanisms in the regulation of adult neurogenesis during stress. *Nature reviews. Neuroscience*, Nature Publishing Group 16(4): 189–200.

Egeland M, Guinaudie C, Du Preez A, Musaelyan K, Zunszain PA, Fernandes C, Pariante CM and Thuret S (2017) Depletion of adult neurogenesis using the chemotherapy drug temozolomide in mice induces behavioural and biological changes relevant to depression. *Translational Psychiatry* 7(4): e1101.

Franklin KBJ and Paxinos G (2012) *The mouse brain in stereotaxic coordinates*. 4th ed. London: Academic Press.

Fava M and Kendler KS (2000) Major depressive disorder. *Neuron* 28(2): 335–41.

Garza JC, Guo M, Zhang W and Lu X-Y (2012) Leptin restores adult hippocampal neurogenesis in a chronic unpredictable stress model of depression and reverses glucocorticoid-induced inhibition of GSK-3β/β-catenin signaling. *Molecular Psychiatry* 17(8): 790–808

Ge JF, Qi CC and Zhou JN (2013) Imbalance of leptin pathway and hypothalamus synaptic plasticity markers are associated with stress-induced depression in rats. *Behavioural Brain Research*, Elsevier B.V. 249: 38–43.

Glover LR, Schoenfeld TJ, Karlsson R-M, Bannerman DM, Cameron HA and Reynolds R (2017) Ongoing neurogenesis in the adult dentate gyrus mediates behavioral responses to ambiguous threat cues. *PLOS Biology* 15(4): e2001154.

Gould TD (2009) Mood and anxiety related phenotypes in mice. Gould TD (ed.), Neuromethods.

Gray JD, Rubin TG, Hunter RG and McEwen BS (2014) Hippocampal gene expression changes underlying stress sensitization and recovery. *Molecular Psychiatry*, Nature Publishing Group 19(11): 1171–1178.

Hains AB, Vu MAT, Maciejewski PK, van Dyck CH, Gottron M and Arnsten AFT (2009) Inhibition of protein kinase C signaling protects prefrontal cortex dendritic spines and cognition from the effects of chronic stress. *Proceedings of the National Academy of Sciences of the United States of America* 106(42): 17957–62.

Hains AB, Yabe Y and Arnsten AFT (2015) Chronic stimulation of alpha-2A-adrenoceptors with guanfacine protects rodent prefrontal cortex dendritic spines and cognition from the effects of chronic stress. *Neurobiology of Stress* 2: 1–9.

Hepgul N, Cattaneo A, Agarwal K, Baraldi S, Borsini A, Bufalino C, Forton DM, Mondelli V, Nikkheslat N, Lopizzo N, Riva MA, Russell A, Hotopf M and Pariante CM (2016) Transcriptomics in Interferon-α-Treated Patients Identifies Inflammation-, Neuroplasticity- and Oxidative Stress-Related Signatures as Predictors and Correlates of Depression. *Neuropsychopharmacology* 41(10): 2502–2511.

Hervé M, Bergon A, Le Guisquet A-M, Leman S, Consoloni J-L, Fernandez-Nunez N, Lefebvre M-N, El-Hage W, Belzeaux R, Belzung C and Ibrahim EC (2017) Translational Identification of Transcriptional Signatures of Major Depression and Antidepressant Response. *Frontiers in Molecular Neuroscience* 10(August): 1–15.

Hinwood M, Tynan RJ, Charnley JL, Beynon SB, Day TA and Walker FR (2013) Chronic stress induced remodeling of the prefrontal cortex: Structural re-organization of microglia and the inhibitory effect of minocycline. *Cerebral Cortex* 23(8): 1784–1797.

Hsu TM, Noble EE, Liu CM, Cortella AM, Konanur VR, Suarez AN, Reiner DJ, Hahn JD, Hayes MR and Kanoski SE (2018) A hippocampus to prefrontal cortex neural pathway inhibits food motivation through glucagon-like peptide-1 signaling. *Molecular Psychiatry* 23(7): 1555–1565.

Hye A, Riddoch-Contreras J, Baird AL, Ashton NJ, Bazenet C, Leung R, Westman E, Simmons A, Dobson R, Sattlecker M, Lupton M, Lunnon K, Keohane A, Ward M, Pike I, Zucht HD, Pepin D, … Lovestone S (2014) Plasma proteins predict conversion to dementia from prodromal disease. *Alzheimer's and Dementia* 10(6): 799–807.

Hornsby AKE, Redhead YT, Rees DJ, Ratcliff MSG, Reichenbach A, Wells T, Francis L, Amstalden K, Andrews ZB and Davies JS (2016) Short-term calorie restriction enhances adult hippocampal neurogenesis and remote fear memory in a Ghsr-dependent manner. *Psychoneuroendocrinology* 63: 198–207.

Jungke P, Ostrow G, Li JL, Norton S, Nieber K, Kelber O and Butterweck V (2011) Profiling of hypothalamic and hippocampal gene expression in chronically stressed rats treated with St. John's wort extract (STW 3-VI) and fluoxetine. *Psychopharmacology* 213(4): 757–772.

Kempermann G (2010) Adult Hippocampal Neurogenesis. 2nd ed. In: *Adult Neurogenesis*, Oxford University Press, pp. 1–85.

Kettner NM, Mayo SA, Hua J, Lee C, Moore DD and Fu L (2015) Circadian dysfunction induces leptin resistance in mice. *Cell Metabolism*, NIH Public Access 22(3): 448–459.

Kim S, Lee S, Ryu S, Suk J and Park C (2002) Comparative analysis of the anxiety-related behaviors in four inbred mice. *Behavioural Processes* 60(2): 181–190.

Krämer A, Green J, Pollard J and Tugendreich S (2014) Causal analysis approaches in Ingenuity Pathway Analysis. *Bioinformatics* 30(4): 523–530.

Kreisel T, Frank MG, Licht T, Reshef R, Ben-Menachem-Zidon O, Baratta M V, Maier SF and Yirmiya R (2014) Dynamic microglial alterations underlie stress-induced depressive-like behavior and suppressed neurogenesis. *Molecular Psychiatry* 19(6): 699–709.

Levkovitz Y, Harel E V, Roth Y, Braw Y, Most D, Katz LN, Sheer A, Gersner R and Zangen A (2009) Deep transcranial magnetic stimulation over the prefrontal cortex: Evaluation of antidepressant and cognitive effects in depressive patients. *Brain Stimulation* 2(4): 188–200.

Li JZ, Bunney BG, Meng F, Hagenauer MH, Walsh DM and Vawter MP (2013) Circadian patterns of gene expression in the human brain and disruption in major depressive disorder. *Proceedings of the National Academy of Sciences of the United States of America* 110: 9950–9955.

Li N, Liu RJ, Dwyer JM, Banasr M, Lee B, Son H, Li XY, Aghajanian G and Duman RS (2011) Glutamate N-methyl-D-aspartate receptor antagonists rapidly reverse behavioral and synaptic deficits caused by

chronic stress exposure. *Biological Psychiatry* 69(8): 754–761.

Lin SM, Du P, Huber W and Kibbe WA (2008) Model-based variance-stabilizing transformation for Illumina microarray data. *Nucleic Acids Research* 36(2): e11.

Liston C, Miller MM, Goldwater DS, Radley JJ, Rocher AB, Hof PR, Morrison JH and Mcewen BS (2006) Stress-Induced Alterations in Prefrontal Cortical Dendritic Morphology Predict Selective Impairments in Perceptual Attentional Set-Shifting. *Journal of Neuroscience* 26(30): 7870–7874.

Liu W, Wang H, Wang Y, Li H and Ji L (2015) Metabolic factors-triggered inflammatory response drives antidepressant effects of exercise in CUMS rats. *Psychiatry Research* 228(3): 257–264.

Liu Y, Yang N and Zuo P (2010) CDNA microarray analysis of gene expression in the cerebral cortex and hippocampus of BALB/c mice subjected to chronic mild stress. *Cellular and Molecular Neurobiology* 30(7): 1035–1047.

Lorenzetti V, Allen NB, Fornito A and Yucel M (2009) Structural brain abnormalities in major depressive disorder: A selective review of recent MRI studies. *Journal of Affective Disorders*, Elsevier B.V. 117(1–2): 1–17.

Malki K, Tosto MG, Pain O, Sluyter F, Mineur YS, Crusio WE, de Boer S, Sandnabba KN, Kesserwani J, Robinson E, Schalkwyk LC and Asherson P (2016) Comparative mRNA analysis of behavioral and genetic mouse models of aggression. *American Journal of Medical Genetics, Part B: Neuropsychiatric Genetics* 171(3): 427–436.

Malki K, Tosto MG, Jumabhoy I, Lourusamy A, Sluyter F, Craig IW, McGuffin P, Schalkwyk LC, Lourdusamy A, Sluyter F, Craig IW, Uher R, McGuffin P, Schalkwyk LC, Lourusamy A, Sluyter F, Craig IW, … Schalkwyk LC (2013) Integrative mouse and human mRNA studies using WGCNA nominates novel candidate genes involved in the pathogenesis of major depressive disorder. *Pharmacogenomics* 14(16): 1979–1990.

Malki K, Mineur YS, Tosto MG, Campbell J, Karia P, Jumabhoy I, Sluyter F, Crusio WE and Schalkwyk LC (2015) Pervasive and opposing effects of Unpredictable Chronic Mild Stress (UCMS) on hippocampal gene expression in BALB/cJ and C57BL/6J mouse strains. *BMC Genomics* 16(1): 262.

Meijering E, Jacob M, Sarria JCF, Steiner P, Hirling H and Unser M (2004) Design and validation of a tool for neurite tracing and analysis in fluorescence microscopy images. *Cytometry. Part A: The Journal of the International Society for Analytical Cytology* 58A(2): 167–176.

Miller BR and Hen R (2015) The current state of the neurogenic theory of depression and anxiety. *Current Opinion in Neurobiology* 30: 51–58.

Morais M, Patrício P, Mateus-Pinheiro A, Alves ND, MacHado-Santos AR, Correia JS, Pereira J, Pinto L, Sousa N and Bessa JM (2017) The modulation of adult neuroplasticity is involved in the mood-improving actions of atypical antipsychotics in an animal model of depression. *Translational Psychiatry*, Nature Publishing Group 7(6): e1146.

Morgan AH, Andrews ZB and Davies JS (2017) Less is more: Caloric regulation of neurogenesis and adult brain function. *Journal of Neuroendocrinology* 29(10): e12512.

Müller HK, Wegener G, Popoli M and Elfving B (2011) Differential expression of synaptic proteins after chronic restraint stress in rat prefrontal cortex and hippocampus. *Brain Research*, Elsevier B.V. 1385: 26–37.

Mutlu O, Gumuslu E, Ulak G, Komsuoglu I, Kokturk S, Maral H, Akar F and Erden F (2012) Effects of fluoxetine , tianeptine and olanzapine on unpredictable chronic mild stress-induced depression-like behavior in mice. *Life Sciences*, Elsevier Inc. 91(25–26): 1252–1262.

Nollet M, Guisquet A Le and Belzung C (2013) Models of Depression: Unpredictable Chronic Mild Stress in Mice. In: *Current Protocols in Pharmacology*, John Wiley & Sons, Inc., pp. 1–17.

Nollet M, Hicks H, McCarthy AP, Wu H, Möller-Levet CS, Laing EE, Malki K, Lawless N, Wafford KA, Dijk D-J and Winsky-Sommerer R (2019) REM sleep's unique associations with corticosterone regulation, apoptotic pathways, and behavior in chronic stress in mice. *Proceedings of the National Academy of Sciences of the United States of America*, National Academy of Sciences 116(7): 2733–2742.

Pawlby S, Hay D, Sharp D, Cerith S W and Pariante CM (2011) Antenatal depression and offspring psychopathology: The influence of childhood maltreatment. *British Journal of Psychiatry* 199(2): 106–112.

Plümpe T, Ehninger D, Steiner B, Klempin F, Jessberger S, Brandt M, Römer B, Rodriguez GR, Kronenberg G and Kempermann G (2006) Variability of doublecortin-associated dendrite maturation in adult hippocampal neurogenesis is independent of the regulation of precursor cell proliferation. *BMC Neuroscience* 7: 77.

Pothion S, Bizot JC, Trovero F and Belzung C (2004) Strain differences in sucrose preference and in the consequences of unpredictable chronic mild stress. *Behavioural Brain Research* 155(1): 135–146.

Potter M (1985) The BALB/c Mouse: Genetics and Immunology. *Current Topics in Microbiology and Immunology*, Springer-Verlag 122: 1–253.

Procaccini C, Aitta-aho T, Jaako-Movits K, Zharkovsky A, Panhelainen A, Sprengel R, Linden A-M and Korpi ER (2011) Excessive novelty-induced c-Fos expression and altered neurogenesis in the hippocampus of GluA1 knockout mice. *The European journal of neuroscience* 33(1): 161–74.

Quennell JH, Howell CS, Roa J, Augustine RA, Grattan DR and Anderson GM (2011) Leptin Deficiency and Diet-Induced Obesity Reduce Hypothalamic Kisspeptin Expression in Mice. *Endocrinology*, Oxford University Press 152(4): 1541–1550.

Schweizer MC, Henniger MSH and Sillaber I (2009) Chronic mild stress (CMS) in mice: Of anhedonia, 'anomalous anxiolysis' and activity. *PLoS ONE* 4(1): e4326.

Slomianka L and West MJ (2005) Estimators of the precision of stereological estimates: An example based on the CA1 pyramidal cell layer of rats. *Neuroscience* 136(3): 757–767.

Spijker S (2011) Neuroproteomics: Dissection of Rodent Brain Regions. *Neuromethods* 57: 13–27.

Srivastava DP, Copits BA, Xie Z, Huda R, Jones KA, Mukherji S, Cahill ME, VanLeeuwen JE, Woolfrey KM, Rafalovich I, Swanson GT and Penzes P (2012) Afadin is required for maintenance of dendritic structure and excitatory tone. *Journal of Biological Chemistry* 287(43): 35964–35974.

Strekalova T, Couch Y, Kholod N, Boyks M, Malin D, Leprince P and Steinbusch HM (2011) Update in the methodology of the chronic stress paradigm: internal control matters. *Behavioral and Brain Functions*, BioMed Central Ltd 7(1): 9.

Sun D (2016) Endogenous neurogenic cell response in the mature mammalian brain following traumatic injury. *Experimental Neurology*, Elsevier Inc. 275: 405–410.

Surget A, Wang Y, Leman S, Ibarguen-Vargas Y, Edgar N, Griebel G, Belzung C and Sibille E (2008) Corticolimbic Transcriptome Changes are State-Dependent and Region-Specific in a Rodent Model of Depression and of Antidepressant Reversal. *Neuropsychopharmacology*, Nature Publishing Group 34(6): 1363–138076.

Surget A and Belzung C (2009) Unpredictable chronic mild stress in mice. In: Kalueff A.V. and LaPorte J.L. (eds), *Experimental Animal Models in Neurobehavioral Research*, New York: Nova Science Publishers, pp. 79–112.

Tusher VG, Tibshirani R and Chu G (2001) Significance analysis of microarrays applied to the ionizing radiation response. *Proceedings of the National Academy of Sciences* 98(9): 5116–5121.

van Tol M, Li M, Metzger CD, Hailla N, Horn DI, Li W, Heinze HJ, Bogerts B, Steiner J, He H and Walter M (2014) Local cortical thinning links to resting-state disconnectivity in major depressive disorder. *Psychological Medicine* 44(10): 2053–2065.

van Zessen R, van der Plasse G and Adan R a. H (2012) Contribution of the mesolimbic dopamine system in mediating the effects of leptin and ghrelin on feeding. *Proceedings of the Nutrition Society* 71(04): 435–445.

Willner P (2005) Chronic mild stress (CMS) revisited: Consistency and behavioural- neurobiological concordance in the effects of CMS. *Neuropsychobiology*, Basel: Karger AG.

Wohleb ES, Fenn AM, Pacenta AM, Powell ND, Sheridan JF and Godbout JP (2012) Peripheral innate immune challenge exaggerated microglia activation, increased the number of inflammatory CNS macrophages, and prolonged social withdrawal in socially defeated mice. *Psychoneuroendocrinology*, Elsevier Ltd 37(9): 1491–1505.

Yuen EY, Wei J, Liu W, Zhong P, Li X and Yan Z (2012) Repeated Stress Causes Cognitive Impairment by Suppressing Glutamate Receptor Expression and Function in Prefrontal Cortex. *Neuron*, Elsevier Inc. 73(5): 962–977.

Zhu X, Li P, Hao X, Wei K, Min S, Luo J, Xie F and Jin J (2015) Ketamine-mediated alleviation of electroconvulsive shock-induced memory impairment is associated with the regulation of neuroinflammation and soluble amyloid-beta peptide in depressive-like rats. *Neuroscience Letters* 599: 32–37.

Zitnik GA, Clark BD and Waterhouse BD (2013) The impact of hemodynamic stress on sensory signal processing in the rodent lateral geniculate nucleus. *Brain Research* 1518: 36–47.

Figure Legends

Figure 1 Behavioural and serological parameters in the UCMS-exposed mice.

Male BALB/cAnNCrl mice (n=10/group) aged 7 weeks at the beginning of the experiment were subjected to UCMS or CNTRL conditions for 6 weeks. (A) Weekly coat state deterioration score measurements from week 4, *p<0.05, **p<0.01 ***p<0.001 derived from Mann-Whitney U-test between CNTRL and UCMS, data represents median and interquartile range; (B) Weekly weight monitoring, *p<0.05 derived from Bonferroni multiple comparison between CNTRL and UCMS group means at week 1 of UCMS; (C) Sucrose consumption measured once every 2 weeks over 2 consecutive nights, **p<0.01 derived from Bonferroni multiple comparisons; (D) Time spent grooming during the splash test; (E) Distance moved during a 5 min exposure to a dimly lit open field; (F) Latency to start eating the pellet in the NSF test; (G) Immobility in the PST; (H) Plasma corticosterone (CORT) response to the PST measured 24 hours before (PRE-PST) and 30 min after (POST-PST) the test; (I) Plasma levels of the C reactive protein (CRP) in the blood collected by the cardiac puncture at the end of the behavioural testing battery (7 days after termination of the UCMS protocol;) (J) Plasma levels of leptin in the blood collected by the cardiac puncture at the end of the behavioural testing battery (7 days after termination of the UCMS protocol). In D-J *p<0.05 **p<0.01, ***p<0.001 derived from two-tailed unpaired t-test, data represents mean±SEM.

Figure 2 Effect of UCMS on the density, morphology and migration of doublecortin-positive (DCX+) neuroblasts and microglial density.

*(*A) Number of neuroblasts residing in the SGZ (0) and in 10 different layers of the granular zone (0.1-1) (GZ); (B) Examples of the DCX+ cells with a high relative migration distance in the hippocampal GZ of the UCMS-exposed mice; (C) Average relative migration distance of DCX+ cell bodies; (D)The density of all DCX+ neuroblasts (TOTAL) and of the "AB", "CD" and "EF" types classified based on their dendritic tree morphology; (E) Examples of AB, CD and EF types of neuroblasts; (F) Representative microphotographs of the Iba1+ cells in the dentate gyrus; (G) Density of the Iba1+ cells in the granular zone (GZ) of the dentate gyrus (DG); (H) Density of Iba1+cells in the medial prefrontal cortex (mPFC) (I) representative microphotographs of Iba1+ cells in the mPFC. Data presented as mean±SEM, *p<0.05, **p<0.01 derived from unpaired t-test CNTRL vs UCMS; #p<0.05 derived from post-hoc Bonferroni multiple comparisons CNTRL vs UCMS

Figure 3 Heatmap of cluster analysis based on the top 500 variable genes.

Adult male BALB/c mice were exposed to unpredictable chronic mild stress (UCMS) or control (CON) for 4 weeks (n=8/group) after which fresh frozen brain tissue from selected brain regions (whole

hippocampus (HIP), hypothalamus (HYP) and prefrontal cortex (PFC)) were subjected to a genome-wide transcriptomic analysis using Illumina microarray platform. The heatmap shows the clustering of samples (top connecting lines) and the heatmap pattern of expression based on intensity values of the top 500 variable genes. The gradient of green and red represents the deviation of each sample intensity value for this gene from the mean intensity across all samples. Individual sample IDs and their groups highlighted at the bottom of the heatmap.

Figure 4 The predicted network of upstream regulators and their target differentially expressed genes in the PFC, designed by the IPA software based on the upstream regulator analysis.

Network of upstream regulators linked to genes differentially expressed in the PFC dataset. The relative size of the upstream regulator molecules reflects their significance ranking with Huntingtin (Htt), Leptin (Lep), myelin regulatory factor (Myrf), methyl-CpG binding protein 2 (Mecp2) and brain derived neurotrophic factor (Bdnf) being the top 5 predicted upstream regulators.

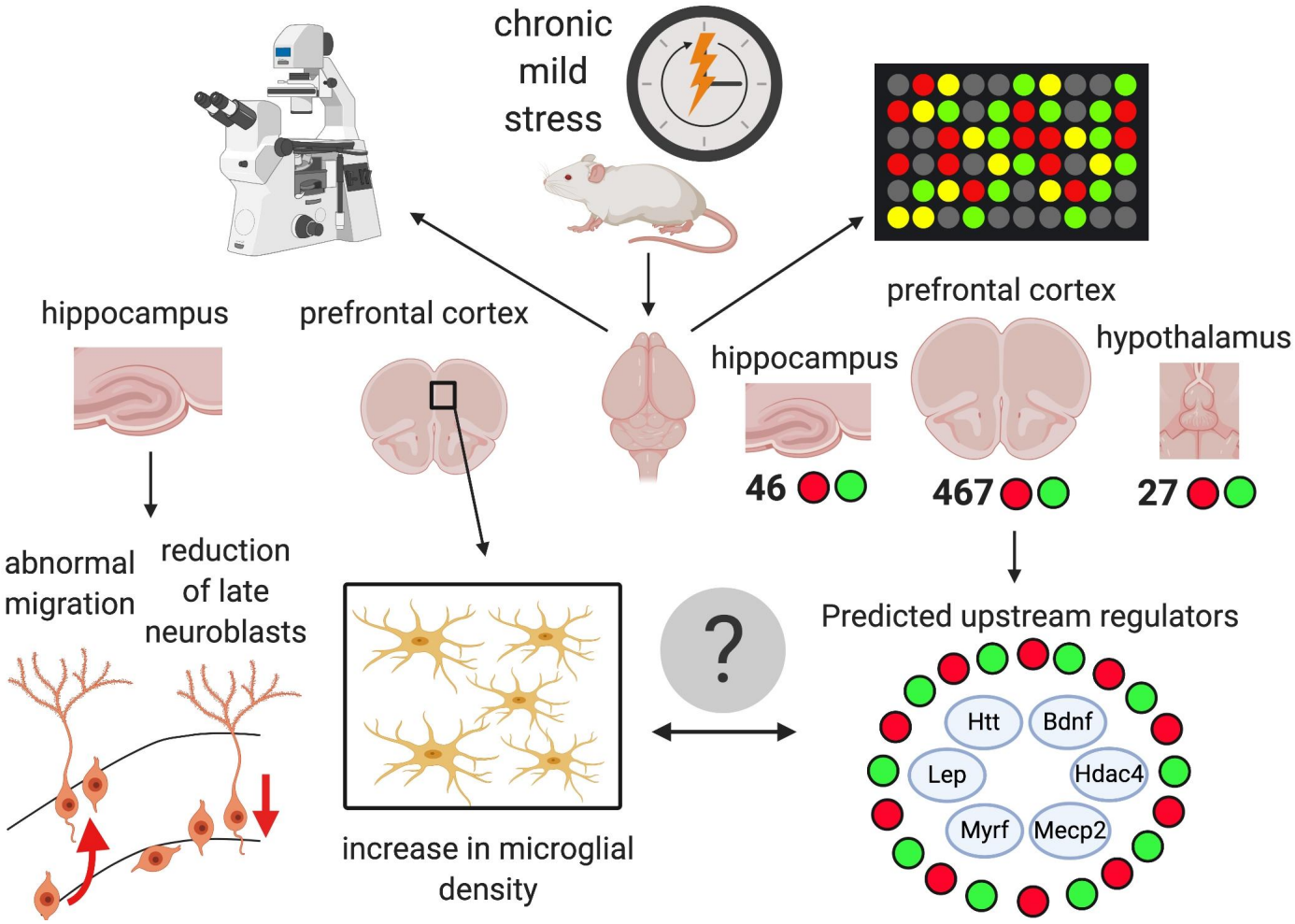
chronic
mild
stress
hippocampus
prefrontal cortex
prefrontal cortex
hippocampus
hypothalamus
46
467
27
abnormal
migration
reduction
of late
neuroblasts
increase in microglial
density
?
Predicted upstream regulators
Htt
Bdnf
Lep
Hdac4
Myrf
Mecp2

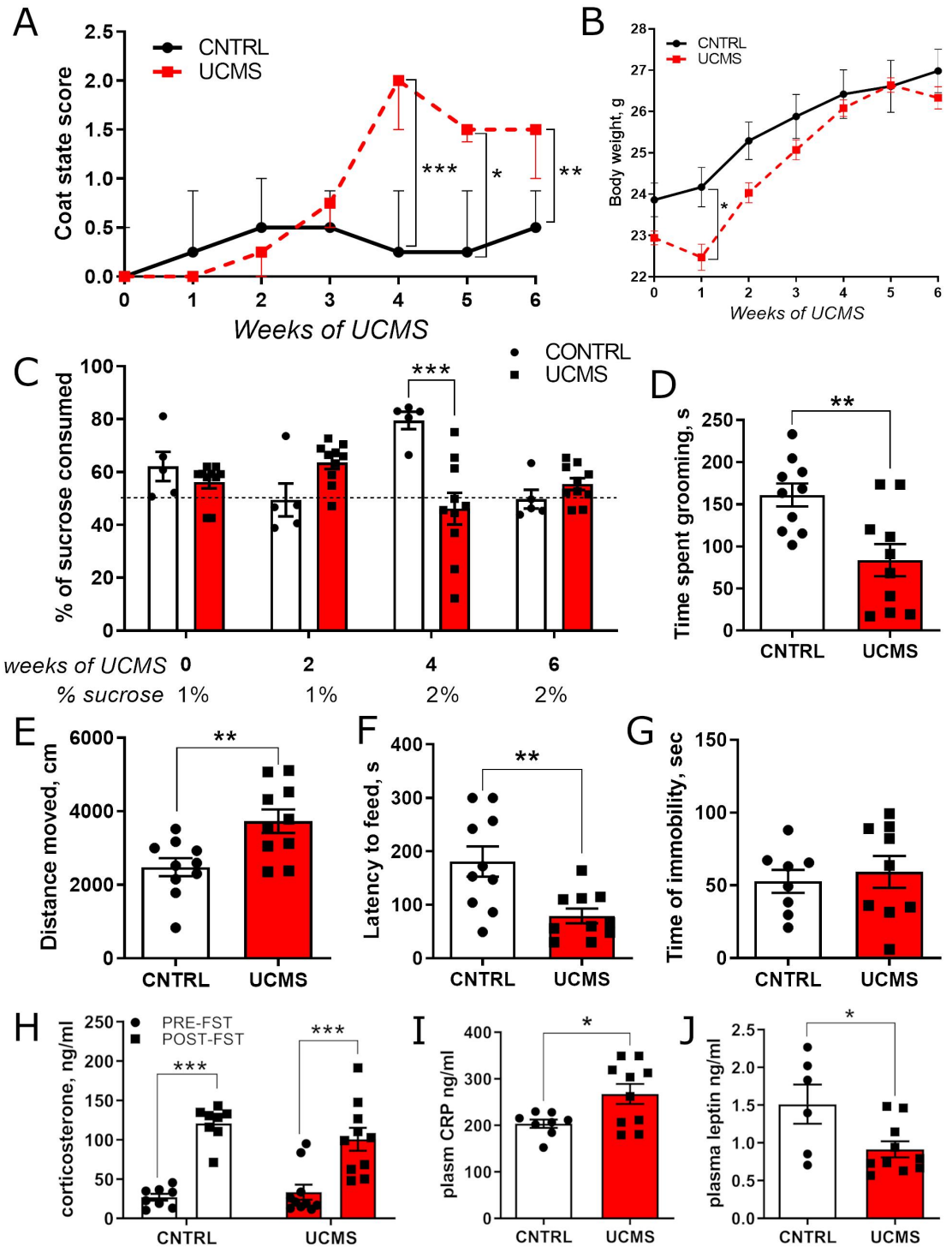
A
Coat state score
CNTRL
UCMS
Weeks of UCMS
B
Body weight, g
CNTRL
UCMS
Weeks of UCMS
C
% of sucrose consumed
CONTRL
UCMS
weeks of UCMS 0 2 4 6
% sucrose 1% 1% 2% 2%
D
Time spent grooming, s
CNTRL
UCMS
E
Distance moved, cm
CNTRL
UCMS
F
Latency to feed, s
CNTRL
UCMS
G
Time of immobility, sec
CNTRL
UCMS
H
corticosterone, ng/ml
PRE-FST
POST-FST
CNTRL
UCMS
I
plasm CRP ng/ml
CNTRL
UCMS
J
plasma leptin ng/ml
CNTRL
UCMS

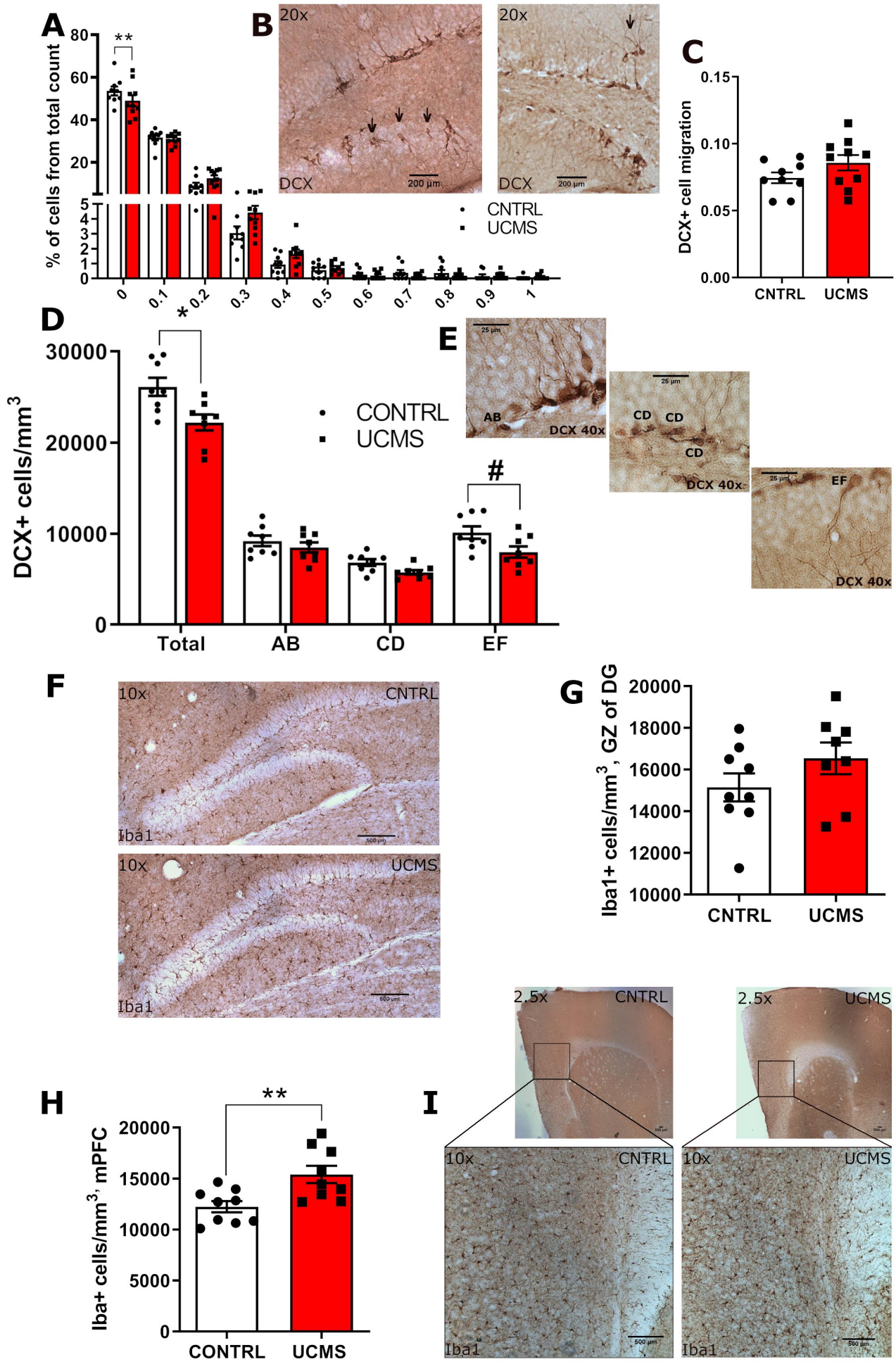
A
B
C
D
E
F
G
H
I
% of cells from total count
CNTRL
UCMS
20x
DCX
200 µm
DCX+ cell migration
0.00
0.05
0.10
0.15
DCX+ cells/mm3
30000
20000
10000
0
Total
AB
CD
EF
25 µm
AB
DCX 40x
CD
EF
10x
Iba1
500 µm
Iba1+ cells/mm3, GZ of DG
20000
18000
16000
14000
12000
10000
2.5x
Iba+ cells/mm3, mPFC
15000
5000

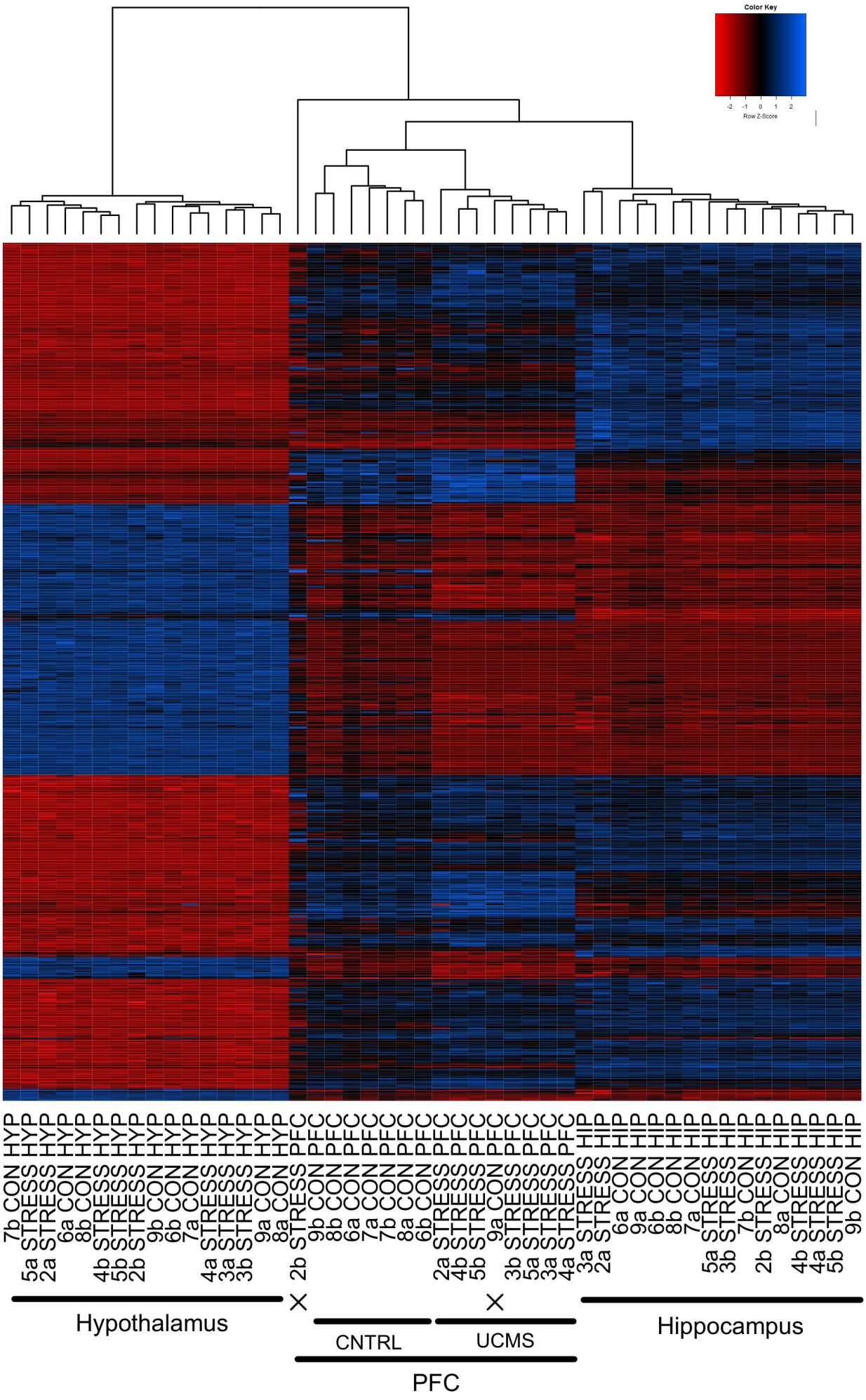
Color Key
-2 -1 0 1 2
Row Z-Score
7b CON HYP
5a STRESS HYP
2a STRESS HYP
6a CON HYP
8b CON HYP
4b STRESS HYP
5b STRESS HYP
2b STRESS HYP
9b CON HYP
6b CON HYP
7a CON HYP
4a STRESS HYP
3a STRESS HYP
3b STRESS HYP
9a CON HYP
8a CON HYP
2b STRESS PFC
9b CON PFC
8b CON PFC
6a CON PFC
7a CON PFC
7b CON PFC
8a CON PFC
6b CON PFC
2a STRESS PFC
4b STRESS PFC
5b STRESS PFC
9a CON PFC
3b STRESS PFC
5a STRESS PFC
3a STRESS PFC
4a STRESS PFC
3a STRESS HIP
2a STRESS HIP
6a CON HIP
9a CON HIP
6b CON HIP
8b CON HIP
7a CON HIP
5a STRESS HIP
3b STRESS HIP
7b CON HIP
2b STRESS HIP
8a CON HIP
4b STRESS HIP
4a STRESS HIP
5b STRESS HIP
9b CON HIP
Hypothalamus
CNTRL
UCMS
Hippocampus
PFC

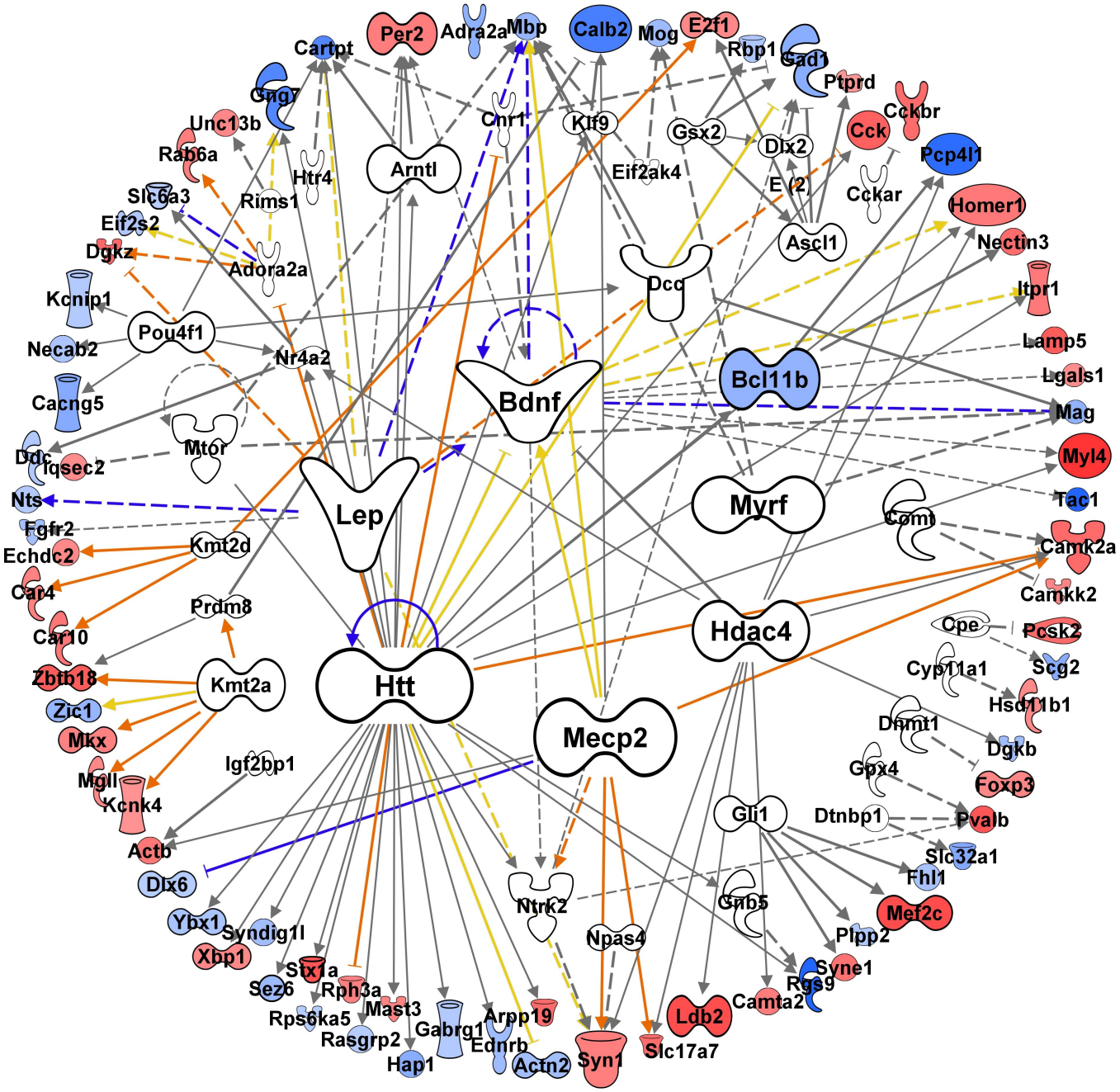
Per2
Adra2a
Mbp
Calb2
Mog
E2f1
Rbp1
Gad1
Cartpt
Ptprd
Cngb1
Cckbr
Unc13b
Cnr1
Klf9
Gsx2
Cck
Dlx2
Pcp4l1
Rab6a
Arntl
Htr4
Eif2ak4
E (2)
Cckar
Slc6a3
Rims1
Homer1
Eif2s2
Ascl1
Nectin3
Dgkz
Adora2a
Dcc
Itpr1
Kcnip1
Pou4f1
Lamp5
Necab2
Nr4a2
Bdnf
Bcl11b
Lgals1
Cacng5
Mag
Mtor
Ddc
Iqsec2
Myl4
Lep
Myrf
Tac1
Nts
Comt
Fgfr2
Kmt2d
Camk2a
Echdc2
Camkk2
Car4
Prdm8
Hdac4
Cpe
Pcsk2
Car10
Htt
Cyp11a1
Scg2
Zbtb18
Kmt2a
Hsd11b1
Zic1
Mecp2
Dnmt1
Mkx
Dgkb
Igf2bp1
Gpx4
Foxp3
Mgll
Kcnk4
Gli1
Dtnbp1
Pvalb
Actb
Slc32a1
Dlx6
Fhl1
Ntrk2
Gnb5
Mef2c
Ybx1
Syndig1l
Npas4
Plpp2
Xbp1
Stx1a
Syne1
Sez6
Rph3a
Rgs9
Rps6ka5
Mast3
Camta2
Arpp19
Ldb2
Rasgrp2
Gabrg1
Ednrb
Slc17a7
Hap1
Actn2
Syn1
Legend
Cytokine/Growth Factor
Growth factor
Ligand-dependent Nuclear Receptor
Transcription Regulator
Transporter
Relationship indirect
no prediction
upregulated
Enzyme
Ion Channel
Peptidase
Translation Regulator
Other
predicted inhibition
effect inconsistent
downregulated
G-protein Coupled Receptor
Kinase
Phosphatase
Transmembrane Receptor
Relationship direct
predicted activation
Colors:

Supplementary methods

Experimental Design

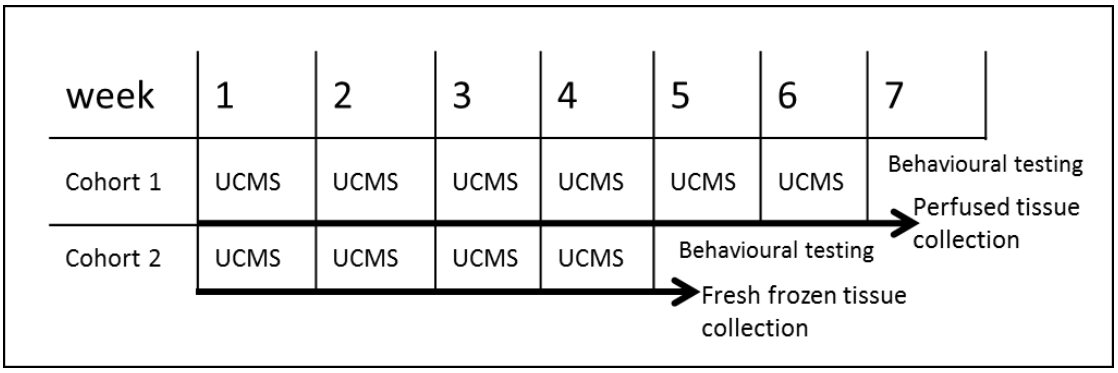

Supplementary Figure 1 Experimental design

Two cohorts of mice were used in this study. Both cohorts consisted of control and UCMS-exposed groups. In cohort 1 (n=10 per group) mice were exposed to stressful or control conditions for 6 weeks, followed by a period of behavioural testing and fixed tissue collection for subsequent immunohistochemistry analysis. In cohort 2 (n=8 per group) mice were exposed to chronic stress or control conditions for 4 weeks, after which their behavioural changes were assessed and fresh frozen tissue was collected for the subsequent gene expression analysis.

Schedule of stressors in the UCMS protocol

Male BALB/cAnNCrl mice aged 8 weeks at the beginning of the experiment were subjected to UCMS or CNTRL conditions for 6 weeks, during which weight, coat state and sucrose preference were monitored weekly. Mice in the CNTRL group were pair-housed with their siblings in large cages (59.5x38x20cm) with environmental enrichment (small plastic and cardboard houses, cardboard tube, paper sizzle nest material; Datesand Ltd, Manchester, UK) to avoid social isolation and minimise home cage aggression in a separate room from the UCMS group area. Mice in UCMS group were single-housed in standard mouse cages (45x28x13cm) with bedding and enrichment provided according to the schedule in Supplementary Table 1.

Day	Stressor 1	Duration	Stressor 2	Duration	Stressor 3	Duration	Stressor 4	Duration
Mon	cage swap	2h	no bedding	2h	new bedding, no enrichment	2h+	new cardboard shelter (no sizzle nest)	over-night
Tue	cage tilt	2h	wet bedding	1,5h	new bedding	2h	predator sounds	30 min
Wed	water bath	30 min	No cardboard shelter	2h	confinement	2h	new house and sizzle nest	over-night
Thu	predator odour	30 min	cage swap	2h	return to cage with intruder's odour	2h	cage tilt	2h
Fri	ruin sizzle nest	n/a	**weight, coat assessment**	n/a	confinement	2 hr	no sizzle nest	1h
Sat	light on/off	4h	light on/off	4h	light on/off	4h	light on/off	4h
Sun	light on/off	4h	light on/off	4h	light on/off	4h	light on/off	4h

Supplementary Table 1 Schedule of stressors used f the UCMS

The following stressors were included in the protocol: tilting of the cage by 45° for a period of 30 min to 3 hours, frequent change of bedding (new bedding), removal of sawdust and minor enrichment for up to 2 hours, exposure to wet sawdust up to 6 hours, exposure to a cage of another mouse in its absence (cage swap) for up to 6 hours, exposure to the odour of intruder mouse after cage swap (return to cage with intruder's odour up to 15 hours (overnight), exposure to predator's odour (Shake Away 2852228 Fox Urine Granules, 15ml per cage) up to 1 hour, exposure to predator's sounds (Birdsong CD (Birds of Prey and Crows), Music Digital 2009) for 30 minutes, replacement of sawdust with 1cm of water at room temperature for 30 minutes (water bath), confinement in a restricted space for up to 1 hour (wire mesh cup 10cm height 8cm diameter alteration of light-dark cycle such as introduction of several intervals of daylight during the night. The schedule was repeated every week for 6 consecutive weeks. After 6 weeks of UCMS exposure mice were subjected to behavioural testing battery, at the end of which blood was collected and mice were culled for brain tissue collection.

Behavioural testing

Sucrose preference (Ducottet and Belzung, 2005) test was conducted using 1 or 2% sucrose solution (Sigma, UK). Prior to testing, all mice were exposed to 2.5% sucrose solution for 1 hour for acclimatisation. Sucrose preference test was conducted during the dark phase over two consecutive

nights. Identical bottles with sucrose or water solutions were placed on either side of a cage lid instead of the regular water bottles with food surrounding the bottles on both sides. To avoid side preference, the location of the bottles on housing cages was switched between the two nights. Bottles were weighted before and after the test to measure liquid consumption. Sucrose preference was calculated using the following formula: Sucrose preference (%) = Vol sucrose / (Vol sucrose + Vol water)*100.

For open field test (Gould, 2009) a circular (40cm diameter) arena was used. During the test the arena was evenly lit with low light (~20 Lux). Behaviours in the arena were video recorded for 10 minutes. For the Novelty-suppressed feeding (NSF) (Dulawa and Hen, 2005) test, mice were food-deprived for 24 hours prior to the test. A large (59.5x38x20cm) novel cage with a thin layer of fresh sawdust was used as a test arena. The standard level of lighting was applied (300 Lux). The food pellet was placed in the middle of the cage on a piece of white cardboard. Mouse behaviour in the test arena was video recorded for 5 min. The latency to feed was measured until the time the mouse started eating the pellet. If the mouse did not touch the pellet during the 5 min, its latency was recorded as 300 sec (less than 3 animals per group). The weight of the pellet before and after the test, as well as after 10 min in the home cage was recorded to measure food intake in a novel and familiar environment. Splash test (Surget and Belzung, 2009) was performed once at the end of the UCMS paradigm according to Nollet *et al*. (2013) in standard lighting conditions (300 Lux). The animals were sprayed with approximately 0.5ml of 10% sucrose solution on the back and transferred to a novel cage devoid of any enrichment. Their latency to start, and time spent, grooming were recorded over 5 min.

For the Porsolt Swim Test, mice were placed in a clear acrylic cylinder filled with 40 cm of water at room temperature for 6 minutes and video was recorded. At the end of the session each mouse was dried using paper towel and returned to home cage. Video recordings were scored manually. An animal was considered to be immobile if passive floating was observed with only movements necessary to keep the head above water. To measure the HPA axis response to the swimming stress, tail vein blood was collected 24 hours before (baseline measure) and 30 min after the test for subsequent corticosterone analysis. For the analysis of all video recordings the automated tracking software EthoVision (Noldus IT, The Netherlands) was used (in automatic or manual mode).

Supplementary table 2 Schedule of behavioural testing.
After 6 weeks of UCMS exposure mice were subjected to behavioural testing battery which included open field test, splash test, novelty suppressed feeding (NSF) and forced swim test (PST) which included blood collection 24 hours before PST (Pre-PST) and 30 min after PST (Post-PST) for corticosterone response measurements.

	TESTING DAY	**DAY1**	**DAY2**	**DAY2**	**DAY3**	**DAY4**	**DAY5**	
N	**GROUP**	**Rest day**	**Open field**	**Splash test**	**NSF**	**Pre-PST blood collection**	**PST**	**Post-PST blood collection**

1	CNTRL		8:58	13:12	14:00	14:20	13:50	14:20
2	UCMS		9:10	13:24	14:07	14:28	13:58	14:28
3	CNTRL		9:22	13:46	14:14	14:36	14:06	14:36
4	UCMS		9:34	13:58	14:21	14:44	14:14	14:44
5	CNTRL		9:46	14:10	14:28	14:52	14:22	14:52
6	UCMS		9:58	14:22	14:35	15:00	14:30	15:00
7	CNTRL		10:10	14:34	14:42	15:08	14:38	15:08
8	UCMS		10:22	14:46	14:49	15:16	14:46	15:16
9	CNTRL		10:34	14:58	14:56	15:24	14:54	15:24
10	UCMS		10:46	15:10	15:10	15:32	15:02	15:32
11	CNTRL		10:58	15:22	15:17	15:40	15:10	15:40
12	UCMS		11:10	15:34	15:24	15:48	15:18	15:48
13	CNTRL		11:22	15:46	15:31	15:56	15:26	15:56
14	UCMS		11:34	15:58	15:38	16:04	15:34	16:04
15	CNTRL		11:46	16:10	15:45	16:12	15:42	16:12
16	UCMS		11:58	16:22	15:52	16:20	15:50	16:20
17	CNTRL		12:10	16:34	15:59	16:28	15:58	16:28
18	UCMS		12:22	16:46	16:06	16:36	16:06	16:36
19	CNTRL		12:34	16:58	16:13	16:44	16:14	16:44
20	UCMS		12:46	17:10	16:20	16:56	16:22	16:52

Brain dissections and RNA extraction

To dissect three brain areas of interest, first the brain was placed with the dorsal side facing down and the hypothalamus was dissected as a rectangle along the lateral border 2 mm from either side of the third ventricle from the optic chiasm to the posterior border of the mammillary bodies, and the thalamus dorsally (Quennell *et al*., 2011). Next the brain was placed with the ventral side facing down and cortex exposed. The cerebral halves were opened out from the midline, after cutting through the corpus callosum. Approximately 3 mm^3 of tissue was cut from the anterior part of the frontal lobes (from 2.46 mm to 1.34 mm relative to bregma (Franklin and Paxinos, 2012), mainly containing the medial prefrontal cortex including some prelimbic cortex, infralimbic cortex, cingulate cortex and motor cortex (Spijker, 2011). For the hippocampal dissection, the cortical hemispheres were peeled

laterally to expose the hippocampus, which was subsequently carefully rolled out with a brush. Whole hippocampi were used for RNA extraction.

Total RNA was extracted from fresh frozen brain tissue by the guanidine isothiocyanate method (Chomczynski and Sacchi, 1987) with TRIzol reagent (Life Technologies, ThermoFisher Scientific Inc.) The quality of the extracted RNA was assessed using 1% agarose gel electrophoresis and spectrophotometry. The 260/280 ratio was over two in all samples indicating a high level of purity in the extracted nucleic acid samples. To remove contaminating DNA from RNA samples DNase digestion of samples was performed using the Qiagen Rnase-Free DNase Set (79254, Qiagen, UK) followed by column-based sample purification using RNeasy MinElute Cleanup Kit (74204, Qiagen, UK), both performed according to the manufacturer's instructions. Subsequently, RNA integrity numbers (RINs) were assessed using the Agilent 2100 Bioanalyzer (G2938-90034, Agilent Technologies, UK) according to the manufacturers' instructions. All samples had RINs of 8.8 or higher, indicating good quality of RNA. RNA concentrations were measured using the Quant-iT™ RiboGreen® RNA assay kit (R11490, ThermoFisher Scientific Inc.) following the manufacturer's instructions

Optical fractionator method

For this analysis an equal number of sections per brain were used. The region of interest (ROI) was delineated under 10x magnification and overlaid with a grid (X=94.6µm, Y=182.5µm) for systematic random sampling. The size of a counting frame was set at 50µmx50µm with 50 desired sampling sites per ROI, according to parameters previously validated for the study of hippocampal neurogenesis (Dias, Bevilaqua, *et al*., 2014). The number of immunopositive cells within each frame was manually counted from the camera image at 40x magnification based on their morphological appearance and position in relation to acceptance and rejection lines of the counting frame (Gundersen, 1977). Subsequently the optical fractionator was applied in the Stereoinvestigator software to estimate the total volume based on the known sections thickness (15µm) and intersection distance (240µm) and cell population by extrapolating the number of cells counted within the counting frames to the total estimated volume of ROI (Slomianka and West, 2005). Subsequently cell density was calculated by diving the estimated population number by the estimated total volume.

DCX cell classification based on dendrite morphology

The DCX positive cells were visually classified according to the categorization of Plumpe *et al*. (2006). The AB group included cells with no, or short, plump processes, most closely resembling the morphology of late type 2b amplifying progenitors, which are already committed to the neuronal lineage as reflected by their DCX expression, yet are still capable of proliferation (Kempermann, 2010); the CD group included cells with medium length processes without branching usually directed along SGZ and not extending beyond the granular zone, most likely representing the cells in transition from

amplifying progenitors to the postmitotic stage of neuronal maturation with first neuritogenesis occurring; the EF group comprised cells with long branching dendrite(s) reaching the molecular layer. These cells are likely to be the type-3 postmitotic progenitors which already receive electrophysiological input (Ambrogini *et al*., 2004).

Microarray and data analysis

Genome-wide gene expression was assessed using the MouseWG-6 BeadChip Kit (Illumina, US), which measures the expression of 45290 transcripts. Sample labelling, hybridisation and signal detection and imaging were performed according to manufacturer's instructions. Briefly 300ng of sample RNA were prepared in 11µl nuclease-free H_20 to be used for labelling and amplification using the Ambion TotalPrep-96 RNA Amplification Kit (4393543, Illumina, US). The concentration of labelled RNA was assessed using Quant-iT™ RiboGreen® RNA assay kit (R11490, ThermoFisher Scientific Inc.) and 1.5ug was loaded onto bead chips for hybridisation. The hybridisation occurred in the Illumina Hybridisation Oven at 58°C for 15 hours 20 min. Next day the beads were washed in high temperature (55°C) buffer and ethanol, and Cy3-Streptavidin was added to bind the beads to allow for signal detection. Finally, laser-induced fluorescent signal from the beads was recorded by iScan System Reader.

Images were analysed using the GenomeStudio software (Illumina, US), where the initial quality control did not detect any outliers based on average signal intensities. Signal intensity data generated by GenomeStudio was pre-processed using the R package Lumi (Du *et al*., 2008). Only transcripts for which intensity values reached the detection threshold of $p<0.01$, and which were expressed in more than 4 samples to allow for individual variation in each treatment group were included into the final statistical analysis (19632 transcripts). Statistical analysis of differential expression was performed using the Statistical Analysis of Microarrays (SAM) method and R-based software (Tusher *et al*., 2001). For PFC data, the user-defined threshold was adjusted to achieve false discovery rate (FDR) of 0 due to a high number of differentially expressed genes. For hippocampal and hypothalamic gene expression, the threshold allowed FDR of 0.095 which corresponds to 0.05% chance of a false-positive finding frequently used in genome-wide gene expression studies (Bagot *et al*., 2016; Malki *et al*., 2016). The dataset for each brain region was analysed separately as a two-class unpaired data.

Microarray validation by quantitative real-time PCR

To verify microarray data analysis, expression of 10 individual genes was independently assessed in the same mRNA samples using real-time quantitative polymerase chain reaction (qPCR). The genes were selected based on their fold changes (a range from the top up- and down-regulated genes to allow for the future correlation analysis with qPCR expression values) and their functional relevance, that is affiliation with one of the top pathways identified to be activated by the pathway analysis

(Myl4, Tnnc, Cam2A, Calb2, Slc32a1, Gad1) or association with chronic stress or depression by the previous studies (Cck, Cckbr, Per2, Gng7).

Reverse transcription of mRNA

For this, firstly mRNA was converted to cDNA by reverse transcription with Superscript III reverse transcriptase (Invitrogen Thermofisher Scientific Inc.) following manufacturer's instructions. Briefly 1µg of mRNA was combined with 250 ng of random hexamer primers (Life Technologies) and 1mM dNTP mix (Thermofisher Scientific Inc.), incubated for 5 minutes at 65°C on a heated block to denature RNA secondary structure and quenched on ice for 1 minute. Next, the following reagents were added to the reaction: 1x First Strand Buffer (Invitrogen), 5 mM dithithretiol (Life Technologies), 40 units RNaseOUT™ (Life Technologies) and 200 units SuperScript III Reverse Transcriptase. Samples were then incubated at 25ºC for 5 minutes, 50ºC for 1 hour, 55ºC for 30 minutes (to remove any secondary structures) and finally 70 ºC for 15 minutes to terminate the reaction.

qPCR primer design

qPCR primers were designed using Integrated DNA Technology (IDT) software (Http://www.idtdna.com/primerquest/home/index) based on target genes DNA sequences obtained from the NCBI Gene database (Http://www.ncbi.nlm.nih.gov/gene). The primers were designed to amplify the exon region targeted by the Beadchip in the microarray. Several conditions were met in primer design: forward and reverse primers were selected to have minimal GC content, similar length, minimal self-complementarity and no complementarity to each other. The length of the amplicon was limited to 70 to 130 base pairs; the amplicon sequence melting temperature was tested for single peak melting curves using uMelt software (Https://www.dna.utah.edu/umelt/umelt.html). The specificity of the primers to the gene of interest was tested in the In silico PCR online software (Http://genome.ucsc.edu/cgi-bin/hgPcr) – only primer pairs replicating a single product from the target gene sequence in the in silico PCR were selected. Specificity was further confirmed by the melting curve analysis – conducted along with the qPCR. Only primer pairs resulting in a single clear peak at predicted temperatures in all tested samples were used for the data. The primer oligonucleotides were synthetized by IDT Custom oligo synthesis service. On arrival, the oligonucleotides were re-suspended in nuclease-free H_20 to a stock concentration of 100 µM and a working concentration of 2 µM. For primer sequences see Supplementary Table 3.

Supplementary Table 3 Primer sequences used for qPCR to validate the gene expression values derived from microarray analysis of RNA collected in the UCMS Experiment 4.
Mouse genome sequences were used for all primers

TARGET GENE	ACCESSION N	AMPLICON LENGTH (bp)	FORWARD PRIMER	REVERSE PRIMER

Myl4	NM_010858.4	103	TCTGGGTAAAGCACGTTTCTC	AGAAGCCATGTGAGTCCAATAC
Tnnc1	NM_009393.2	82	CCGTGGTAGGAGTGCAG	GGAGAGAAAGTCCGGAAGG
Cck	NM_001284508.2	85	GGAGGTGGAATGAGGAAACAA	GCACACTCTGGACAGATTTCA
Camk2a	NM_009792.3	102	CATCCTGAACCCTCACATCC	GCATCCAGGTACTGAGTGATG
Cckbr	NM_007627.5	94	TCTATAGTGCCCATAGCCTAGT	TTCAGTGCTGGATAAGGAAGG
Per2	NM_011066.3	94	GTAACAGGGAAGCCACAAGAG	TGAGAGGATGTCAGGAGAGATG
Calb2	NM_007586.1	75	GTGGATCTGGAAAGGAGAGATG	CGCAGGCACAACTGTCTAT
Gng7	NM_001038655.1	97	CCTTCCCTCTGCTTTGTGAA	CAATAGTAACACTGGGAGAGTGG
Slc32a1	NM_009508.2	116	GCGTTTCTGTCGTCCTTTCT	TTTGGTGGTGGTGGTGATG
Gad1	NM_008077.5	102	CCCTCTTTACAGAACCAGAATCA	CTTCAGTGAGATGGCCTAGATG
Atp5b	NM_016774.3	92	GCTGATAAGCTGGCAGAAGA	CCTGAGCTCTCGCTTGATATG
Cst3	NM_009976.4	97	GACTGACTGTCCTTTCCATGAC	CAGGGAGTGTGTGCCTTTC

qPCR and its data analysis

qPCR reaction master mix was assembled in white 96 well qPCR plates (AB-0900/W, ThermoFisher Scientific Inc.). All samples assayed for the same gene were included on the same plate. The master mix consisted of 5x HOT FIREPol® EvaGreen® qPCR Mix Plus (no ROX) (Solis BioDyne), containing DNA polymerase which incorporates EvaGreen fluorescent dye into double-stranded DNA; 0.2µM forward and reverse primer mix and nuclease-free water. cDNA template (31.25ng) or water was added to the duplicate wells. The reaction was performed on a Chromo4 Real-time PCR detector (Bio-Rad Laboratories Inc.) according to the following programme: initial denaturation at 95°C for 15 minutes, 45 cycles of denaturation at 95°C for 30 seconds, annealing at 60°C for 30 seconds, extension at 72°C for 30 seconds. Fluorescent signal was detected at the end of each cycle. At the end of the protocol a melting curve analysis was carried out by detecting the fluorescence during a heating step from 60°C to 95°C at every 1°C increment.

Data was extracted with Opticon Monitor 3 (Bio-Rad Laboratories Inc.) software. To calculate relative gene expression, cycle threshold (Ct) values for target genes were normalised to the reference genes Atp5b and Cst3, and expression ratio was calculated separately for each UCMS group sample relative to the average value of all CNTRL group samples using the Pfaffl mathematical model (see Equation 1) according to Pfaffl *et al*., 2001.

$$\boldsymbol{Ratio} = \frac{\boldsymbol{E\,target}^{\boldsymbol{\Delta Ct(control-sample)}}}{\boldsymbol{E\,ref}^{\boldsymbol{\Delta Ct(control-sample)}}}$$

Equation 1 Pfaffl mathematical model used to quantify relative expression of target genes in the qPCR, where E target is efficiency of a target gene and E ref is efficiency of a reference gene; ΔCt was calculated by subtraction of the Ct value of a replicon of each UCMS group sample ("sample") from average Ct of this gene in all CNTRL group samples ("control")

For this analysis, 2 reference genes were selected based on low variation and high expression levels in the microarray dataset across all samples and regions accessed, as the reference gene is required to have a stable level of expression independent of treatment exposure. The variation of a gene's expression was estimated by calculating its CV in all samples. Among genes with low CV only genes with high levels of expression (intensity values ≥12 in all samples across all tissues) were considered for reference role to ensure stable PCR results. Based on these two parameters, Atp5b and Cst3 emerged as reasonable candidates. Moreover, Atp5b has been previously validated as a suitable reference gene for gene expression analysis in a mouse brain (Cleal *et al.*, 2014), therefore these two genes were used as reference genes in the Pfaffl equation.

The average of ratios normalised to the two reference genes were used in statistical analysis. Average group ratio for each gene was compared to the relative control expression level set at 1 with a 1-sample t-test. To compare the expression values derived from the microarray from those obtained with a qPCR, Pearson's correlation has been conducted between microarray values for each target gene and corresponding qPCR-derived group average gene expression ratios.

Supplementary data

Behavioural characteristics of the Cohort 2 used for gene expression were similar to that of the UCMS cohort 1 described above

To confirm the presence of behavioural changes in the UCMS cohort used in the gene expression study, mice were subjected to selected behavioural tests from the testing battery prior to fresh frozen tissue collection. UCMS induced deterioration of the coat state and reduction of grooming in the splash test in the exposed mice, although in this cohort the onset of effect occurred already after one week of UCMS exposure (Mann-Whitney U = 45, p>0.995 on week 0; U = 3, p = 0.0002 on week 1; U=5, p = 0.0003 on week 2; U=5, p=0.0002 on week 3; U=28.5 p = 0.181 on week 4) (see Supplementary Figure 2A). Changes in coat state were not accompanied by group differences in weight (see Supplementary Figure 2B). Unlike the UCMS Cohort 1, UCMS-exposed group in Cohort 2 did not display differences in the locomotor activity measured by distance travelled in the open field arena (see Supplementary Figure 2A). However similarly to the Cohort 1, UCMS-exposed mice showed reduction of grooming time (Mann-Whitney U = 10, p = 0.003) in the splash test (see Supplementary Figure 2D).

Interestingly in this experiment similarly to the Cohort 1 mice displayed weekly fluctuation of preference for sucrose. However unlike in the previous experiment, in Cohort 2 anhedonia was

detected already after 1 week of the UCMS exposure. However, upon repeated exposures to the same sucrose concentration (1%) the preference fluctuated during subsequent weeks, with UCMS group preference being significantly higher than the CNTRL group preference on week 3 (see Supplementary Figure 2C). These cohort differences in sucrose response could be explained by the frequency of sucrose preference testing, with more frequent sucrose exposure in the 4-week cohort inducing a craving-type response in stressed group, where preference for sucrose was higher than water on weeks two to four. In the novelty suppressed feeding test, UCMS group showed reduced latency to start eating the food pellet in the middle of the novel arena, identical to that observed in the cohort 1 (see Supplementary Figure 2F).

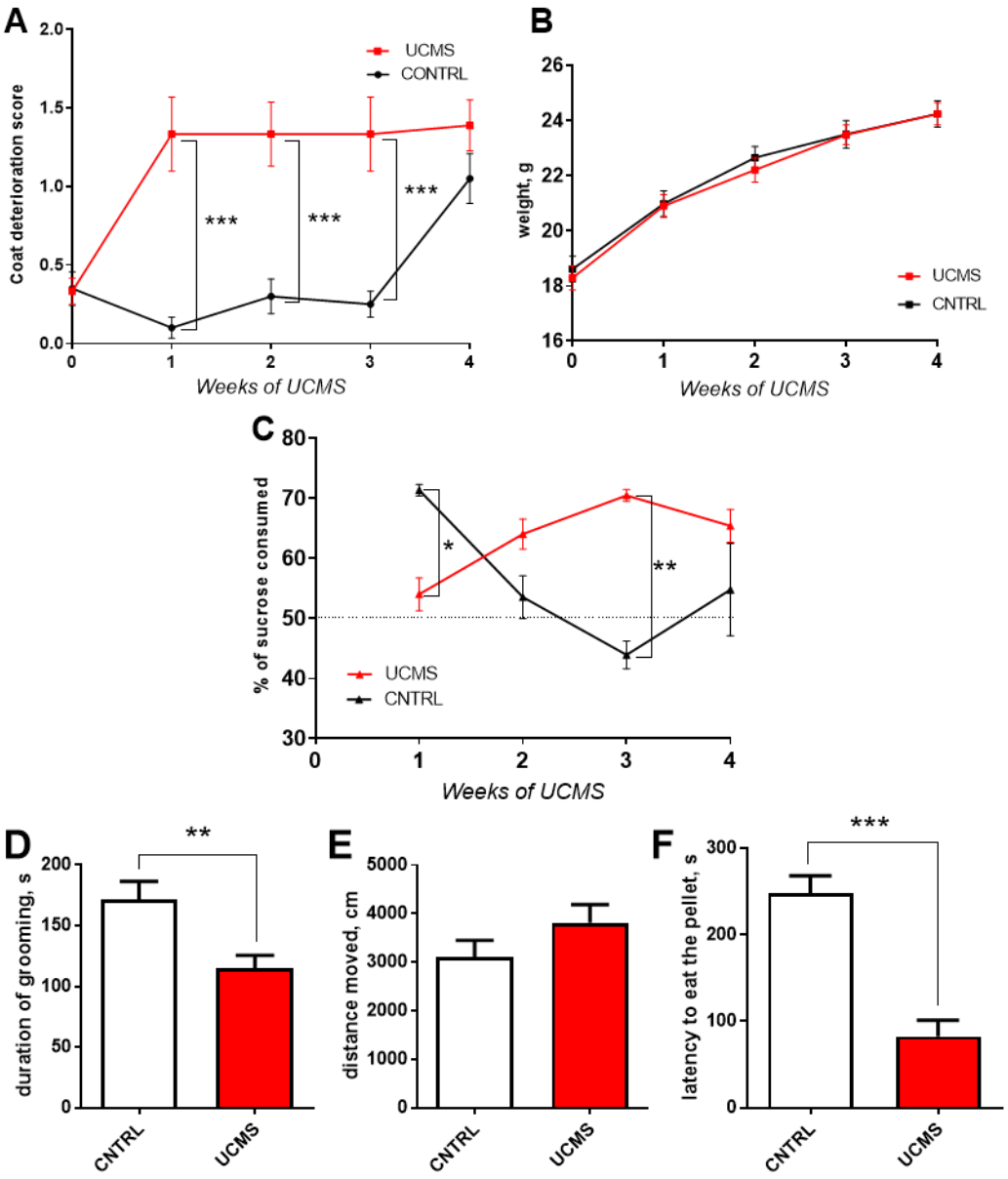

*Supplementary Figure 2 Weekly measures of coat state, weight change and sucrose preference in the UCMS Cohort 2 weekly weight measures in UCMS and CNTRL groups (B) weekly coat state measures in UCMS and CNTRL groups (C) average weekly sucrose preference measures taken over 2 consecutive nights to allow for sucrose bottle side change; (D) duration of grooming in the 5 min splash test (E) locomotion on the open field test (F) latency to start eating the pellet in the NSF test; *p<0.05, **p<0.01, ***p<0.001 CNTRL vs UCMS derived from Mann-Whitney U-test (coat state), post-hoc Bonferroni multiple comparisons (sucrose preference) or t test (D-F). Data represents mean ± SEM, n=8/group*

qPCR data replicated the microarray analysis for 10 genes selected from the PFC dataset

10 genes selected from the top differentially expressed genes in the PFC have been also measured using qPCR to validate the results of the microarray analysis. The average UCMS group relative

expression of all 10 selected genes calculated against the expression of two reference genes Apt5b and Cst3 significantly differed from CNTRL (see Supplementary Figure 4A). Moreover, relative expression values showed a strong correlation with fold change data derived from the microarray analysis (see Supplementary Figure 4B).

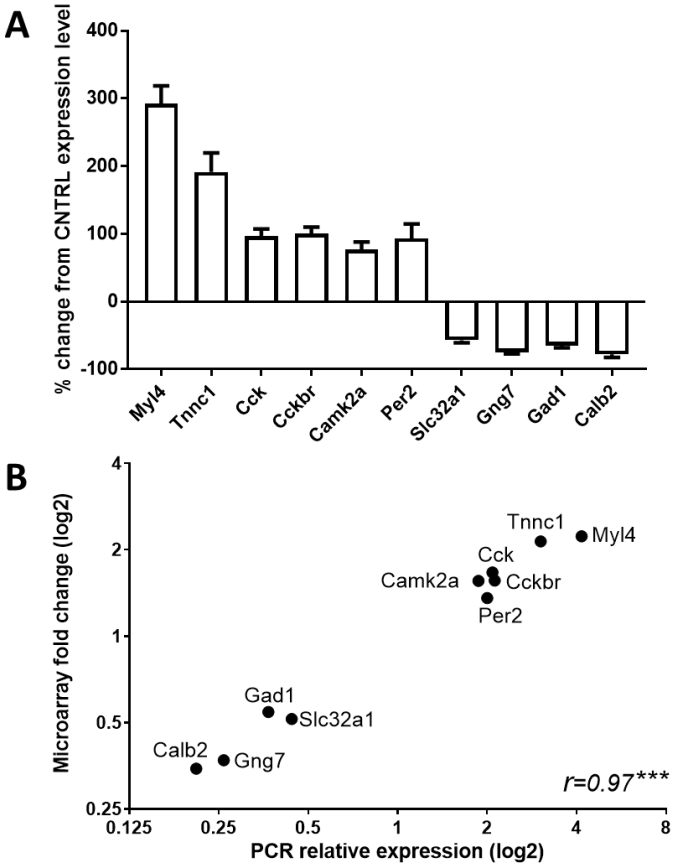

Supplementary Figure 3 Validation of microarray analysis by qPCR gene expression data

Adult male BALB/c mice were exposed to unpredictable chronic mild stress or control for 4 weeks (n=8/group) after which fresh frozen brain tissue from selected brain regions (hippocampus (HIP), hypothalamus (HYP) and prefrontal cortex (PFC)) were subjected to a genome-wide transcriptomic analysis using Illumina microarray platform. (A) Relative gene expression of 10 genes selected from the list of significantly differentially expressed genes in the microarray was evaluated using qPCR by Pfaffl method, normalised to the expression of 2 housekeeping genes Atp5b and Cst3. Average relative expression of each gene was significantly different from the control level ($p<0.05$ for all genes, derived from 1-sample t-test) (B) For the 10 genes selected for validation by qPCR, there was a strong correlation between the microarray (Y axis) and qPCR (X axis) – derived relative expression levels (Pearson's $r=0.97$, $p***<0.001$).

Statistical Analysis of Microarrays (SAM)

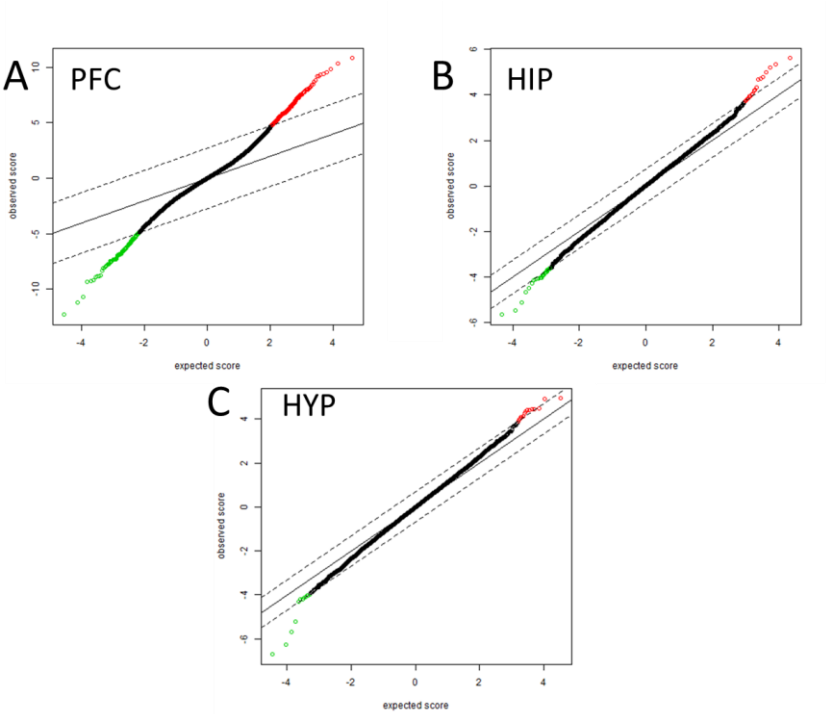

Supplementary Figure 4 SAM plot of differentially expressed genes in the PFC (A), the hippocampus (B) and the hypothalamus (C).

Plot of the expected (X axis) vs observed (Y axis) relative difference in expression of individual genes between CNTRL and UCMS conditions (n=8/group) shows genes for which this relationship deviates from the equality line beyond the set threshold of false discovery rate (ΔFDR, broken line). FDR of 0 yielded 467 genes significantly increased (in red) or decreased (in green) in the PFC; FDR 0.095 yielded 46 significant genes in HIP and 27 significant genes in HYP. Hippocampus (HIP), hypothalamus (HYP), prefrontal cortex (PFC).

Supplementary Data tables

Supplementary Table 4 Top up and downregulated genes based on fold change estimation (1.5 and above fold increase and 0.65 fold an below decrease) derived from SAM and annotated by Ingenuity based on Entrez gene database.

TOP UPREGULATED GENES IN THE PFC				TOP DOWNREGULATED GENES IN THE PFC		
	GENE	Fold Change	Entrez gene name	GENE	Fold change	Entrez gene name
1	Myl4	2.232	Myosin, light chain 4	Rgs9	0.285	Regulator of G-protein signalling 9
2	Tnnc1	2.149	Troponin C type 1 (slow)	Tac1	0.286	Tachykinin, precursor 1
3	Nrgn	2.071	Neurogranin	Pcp4l1	0.304	Purkinje cell protein 4-like 1
4	C17orf96	2.063	Chromosome 17 open reading frame 96	Calb2	0.346	Calbindin 2
5	Fezf2	2.019	FEZ family zinc finger 2	Cartpt	0.368	CART prepropeptide
6	Cpne9	1.965	Copine family member IX	Gng7	0.373	Guanine nucleotide binding protein (G protein), gamma 7
7	Mef2c	1.878	Myocyte enhancer factor 2C	Cartpt	0.481	CART prepropeptide
8	Dkk3	1.869	Dickkopf WNT signaling pathway inhibitor 3	Slc32a1	0.515	Solute carrier family 32 (GABA vesicular transporter), member 1
9	Ldb2	1.864	LIM domain binding 2	Chn2	0.521	Chimerin 2
10	Satb1	1.817	SATB homeobox 1	Cacng5	0.526	Calcium channel, voltage-dependent, gamma subunit 5
11	Stx1a	1.785	Syntaxin 1A (brain)	Lmo3	0.538	LIM domain only 3
12	Pvalb	1.765	Parvalbumin	Scg2	0.541	Secretogranin II
13	Nfix	1.737	Nuclear factor I/X (CCAAT-binding transcription factor)	Gad1	0.545	Glutamate decarboxylase 1 (brain, 67kda)

TOP UPREGULATED GENES IN THE PFC				TOP DOWNREGULATED GENES IN THE PFC		
	GENE	Fold Change	Entrez gene name	GENE	Fold change	Entrez gene name
14	9130024f11rik	1.721	RIKEN cdna 9130024F11 gene	Hap1	0.547	Huntingtin-associated protein 1
15	Zbtb18	1.715	Zinc finger and BTB domain containing 18	Apod	0.560	Apolipoprotein D
16	Lamp5	1.708	Lysosomal-associated membrane protein family, member 5	Slc17a6	0.561	Solute carrier family 17 (vesicular glutamate transporter), member 6
17	Cck	1.672	Cholecystokinin	Gad1	0.569	Glutamate decarboxylase 1 (brain, 67kda)
18	Galnt9	1.648	Polypeptide N-acetyl-galactosaminyltransferase 9	Tf	0.570	Transferrin
19	Arhgap32	1.632	Rho gtpase activating protein 32	Zcchc12	0.571	Zinc finger, CCHC domain containing 12
20	Ccl27a	1.627	Chemokine (C-C motif) ligand 27A	Pcp4l1	0.573	Purkinje cell protein 4-like 1
21	Ddit4l	1.584	DNA-damage-inducible transcript 4-like	Adra2a	0.577	Adrenoceptor alpha 2A
22	Tex40	1.584	Testis expressed 40	Mobp	0.581	Myelin-associated oligodendrocyte basic protein
23	Sytl2	1.576	Synaptotagmin-like 2	Tiam1	0.587	T-cell lymphoma invasion and metastasis 1
24	Dgkz	1.574	Diacylglycerol kinase, zeta	Bcl11b	0.592	B-cell CLL/lymphoma 11B (zinc finger protein)
25	Tshz3	1.568	Teashirt zinc finger homeobox 3	Tpbg	0.593	Trophoblast glycoprotein
26	Camk2a	1.565	Calcium/calmodulin-dependent protein kinase II α	Mag	0.594	Myelin associated glycoprotein
27	Pcsk2	1.561	Proprotein convertase subtilisin/kexin type 2	Ppp1r2	0.596	Protein phosphatase 1, regulatory (inhibitor) subunit 2
28	Osbpl1a	1.550	Oxysterol binding protein-like 1A	Strip2	0.598	Striatin interacting protein 2

	TOP UPREGULATED GENES IN THE PFC			TOP DOWNREGULATED GENES IN THE PFC		
	GENE	Fold Change	Entrez gene name	GENE	Fold change	Entrez gene name
29	Nuak1	1.547	NUAK family, SNF1-like kinase, 1	Meis1	0.600	Meis homeobox 1
30	Arpp19	1.544	Camp-regulated phosphoprotein, 19kda	Cacng5	0.604	Calcium channel, voltage-dependent, gamma subunit 5
31	Cckbr	1.539	Cholecystokinin B receptor	Mbp	0.606	Myelin basic protein
32	Mapk11	1.538	Mitogen-activated protein kinase 11	Zic1	0.612	Zic family member 1
33	Pvrl3	1.537	Poliovirus receptor-related 3	Clic6	0.617	Chloride intracellular channel 6
34	Cobl	1.529	Cordon-bleu WH2 repeat protein	H3f3a/H3f3b	0.626	H3 histone, family 3A
35	Slc17a7	1.528	Solute carrier family 17 (vesicular glutamate transporter), member 7	Btg1	0.634	B-cell translocation gene 1, anti-proliferative
36	Ccdc3	1.522	Coiled-coil domain containing 3	Tmem255a	0.638	Transmembrane protein 255A
37	Arhgef25	1.514	Rho guanine nucleotide exchange factor (GEF) 25	Cntnap2	0.650	Contactin associated protein-like 2
38	Extl1	1.508	Exostosin-like glycosyltransferase 1	Sez6	0.650	Seizure related 6 homolog (mouse)

Supplementary Table 5 Differentially expressed genes in the hippocampus and the hypothalamus

THE HIPPOCAMPUS UPREGULATED GENES			**THE HYPOTHALAMUS UPREGULATED GENES**		
Gene name	**Fold change**	**Q-value (%)**	**Gene name**	**Fold change**	**Q-value (%)**
Mkks	1.17	0.00	C330006p03rik	1.10	4.99
Per2	1.26	0.00	Uhrf2	1.21	4.99
Mfsd2	1.22	0.00	Camk1	1.13	4.99
Zfp207	1.13	0.00	Tsc22d3	1.12	4.99
Htra1	1.21	0.00	Htra1	1.22	4.99
1110057k04rik	1.15	0.00	Mfsd2	1.22	4.99
Nrp1	1.14	0.00	Loc634015	1.15	4.99
1190003m12rik	1.07	0.00	Mrrf	1.12	4.99
Arpc2	1.30	5.83	Fam107a	1.29	4.99
Pglyrp1	1.06	6.03	Chic1	1.04	4.99
C1ql3	1.11	6.03	Agxt2l1	1.18	4.99
1190005n23rik	1.10	6.03	Copg	1.17	4.99
Fam13c	1.10	6.03	C2	1.07	4.99
Tsc22d3	1.18	9.51	Loc665506	1.07	4.99
Sh3md4	1.05	9.51	Dusp19	1.11	9.97
S3-12	1.08	9.51			
Hace1	1.13	9.51			
Smox	1.14	9.51			
THE HIPPOCAMPUS DOWNREGULATED GENES			**THE HYPOTHALAMUS DOWNREGULATED GENES**		
Gene name	**Fold change**	**Q-value (%)**	**Gene name**	**Fold change**	**Q-value (%)**
Bex4	0.90	0.00	Klhdc9	0.88	0.00

B230373p09rik	0.88	0.00	Loc385256	0.85	0.00
Hnrpdl	0.82	0.00	Nrxn2	0.88	0.00
Loc100047427	0.89	0.00	Hdgfrp2	0.83	0.00
Hint2	0.84	5.83	Gm129	0.94	9.97
Klhdc9	0.85	5.83	Pcdh19	0.92	9.97
Pllp	0.89	7.61	Vangl2	0.92	9.97
Asphd1	0.90	7.61	Cacng5	0.91	9.97
Sgcb	0.91	7.61	Dgat2	0.86	9.97
Dcx	0.95	7.61	Loc100047427	0.88	9.97
Tmem86a	0.92	7.61	Mbtps1	0.89	9.97
Mrps28	0.90	7.61	Rab34	0.88	9.97
0610007p22rik	0.81	7.61			
Slc4a3	0.88	7.61			
Hyal2	0.93	7.61			
Zfp46	0.85	7.61			
Haghl	0.85	10.29			
Krt1-12	0.89	10.29			
Blmh	0.88	10.29			
Gucy1a3	0.82	10.29			
Lmnb1	0.92	10.29			
Cyp4f13	0.95	10.29			
Wbp5	0.89	10.29			
Nr1d1	0.93	10.29			
Gdf10	0.90	10.29			
Setd5	0.89	10.29			
Ai836003	0.91	10.29			